SLAC-PUB-6276
June 1993
(E/I)

PERFORMANCE of the CRID at SLD*

K. Abe,[a] P. Antilogus,[b] D. Aston,[b] K. Baird,[c] A. Bean,[d] R. Ben-David,[e] T. Bienz,[b] F. Bird,[b] D. O. Caldwell,[d] M. Cavalli-Sforza,[f] J. Coller,[g] P. Coyle,[f] D. Coyne,[f] S. Dasu,[b] S. Dolinsky,[b] A. d'Oliveira,[h] J. Duboscq,[d] W. Dunwoodie,[b] G. Hallewell,[b] K. Hasegawa,[a] Y. Hasegawa,[a] J. Huber,[d] Y. Iwasaki,[a] P. Jacques[c] R. A. Johnson,[h] M. Kalelkar,[c] H. Kawahara,[b] Y. Kwon,[b] D.W.G.S. Leith,[b] X. Liu,[f] A. Lu,[d] S. Manly,[e] J. Martinez,[h] L. Mathys,[d] S. McHugh,[d] B. Meadows,[h] G. Müller,[b] D. Muller,[b] T. Nagamine,[a] M. Nussbaum,[h] T. J. Pavel,[b] R. Plano,[c] B. Ratcliff,[b] P. Rensing,[b] A. K. S. Santha,[h] D. Schultz,[b] J. T. Shank,[g] S. Shapiro,[b] C. Simopoulos,[b] J. Snyder,[e] M.D. Sokoloff,[h] E. Solodov,[b] P. Stamer,[c] I. Stockdale,[h] F. Suekane,[a] N. Toge,[b] J. Turk,[e] J. Va'vra,[b†] J. S. Whitaker,[g] D. A. Williams,[f] S. H. Williams,[b] R. J. Wilson,[i] G. Word,[c] S. Yellin,[d] H. Yuta[a]

[a]Department of Physics, Tohoku University, Aramaki, Sendai 980, JAPAN
[b]Stanford Linear Accelerator Center, Stanford, CA 94309, USA
[c] Serin Physics Laboratory, Rutgers University, P.O. Box 849, Piscataway, NJ 08855, USA
[d]Department of Physics, University of California, Santa Barbara, CA 93106, USA
[e]Department of Physics, Yale University, New Haven, CT 06511, USA
[f]Santa Cruz Inst. for Particle Physics, University of California, Santa Cruz, CA 95064, USA
[g]Department of Physics, Boston University, Boston, MA 02215, USA
[h]Department of Physics, University of Cincinnati, Cincinnati, OH 45221, USA
[i]Department of Physics, Colorado State University, Fort Collins, CO 80523, USA

Abstract

This paper describes the performance of a large 4π Cherenkov Ring Imaging Detector (CRID) in the SLD experiment at the SLC at SLAC. We compare the most recent SLD results with those obtained during the R&D period, discuss various design features, and highlight some specific lessons derived from three years of operation.

---

† Speaker—Invited talk at the First Workshop on Rich Detectors, Bari, Italy, June 2-6, 1993.

*Work supported by Department of Energy contract DE-AC03-76SF00515

Invited talk at the First Workshop on Ring Imaging Cherenkov Detectors (Rich 93),
Bari, Italy, June 2-5, 1993

1. INTRODUCTION

The concept of the CRID at SLD benefited from the pioneering work of J. Seguinot and T. Ypsilantis.[1] The design is similar to that of the DELPHI[2] RICH and both groups benefited from each other's work. The early R&D development of CRID was summarized in ref.3.

In this paper we describe the performance of the barrel portion of the CRID detector. By making use of both liquid and gaseous radiators in the Barrel CRID, π/K/p separation will be possible up to about 30 GeV/c, and e/π separation up to about 6 GeV/c.

2. CRID DESIGN FEATURES

Fig.1 shows the basic CRID geometry, and more detail about its electrostatic design can be found in ref.4. The CRID includes 40 TPC's, 40 liquid radiator trays containing liquid C_6F_{14}, a vessel containing 76% C_5F_{12}+24% N_2 gas radiator, and a system of 400 spherical mirrors.[5] The Cherenkov photons are focused into the TPC's as shown in Fig.2. The photoelectron drifts to a wire chamber where its position is reconstructed using a combination of drift time (z-coordinate), wire address (x-coordinate) and charge division (y-coordinate) with a precision of 1x1x2 mm. The expected Cherenkov angles are 3.04° and 38.5° (β = 1 particle) with expected resolutions of 4-5 and 12-15 mrad for gas and liquid rings respectively, and on average 7-9 and 13 -16 photoelectrons are expected on gas and liquid rings respectively - see chapter 3.11 for N_o estimate. The TPC gas is C_2H_6+ TMAE(~0.1%). The maximum drift length is 1.2 m, and the maximum operating voltage is 55 kV giving a drift field of 400 V/cm. The system operates at 33-35°C with the TMAE bubbler temperature set at 26°C. The system has 3720 anode wires, 7440 amplifiers, 64000 field shaping electrodes and 6520 corona preventing field wires.

We are presently commissioning the End Cap portion of the CRID which will be described in a future publication. It will operate with a C_4F_{10} gas radiator only, and includes 10 TPC's and 120 mirrors. The TPC gas is 85% C_2H_6+15% CO_2+TMAE(~0.1%); the maximum drift length is 28 cm; and the maximum voltage is 15 kV, giving a 400 V/cm drift field. The system has 1280 anode wires.

3. REVIEW OF THE SYSTEM PERFORMANCE

3.1. Overall experience

Here, we highlight a few major issues where we differ from other CRID/RICH devices now in operation.

To define the drift field in the TPC's we decided to use a simple geometry with field cage wires rather than a volume degrader. Our experience so far at SLD with the high voltage is excellent indicating that it is not necessary to build a volume degrader for voltages up to 60 kV and distances of 8-10 cm to ground, provided that a gas with good dielectric properties fills the volume.

We also decided to require that the detectors be easily removable for repairs. However, it is well known that TMAE attacks most elastomers. Our choice of Viton O-rings[6] has proven to be satisfactory. After 3 years of TMAE operation, we have not seen any deterioration of the O-ring.

The electrodes on two sides of the TPC were made of G-10 with copper traces. It was necessary to coat the G-10 surface with a TMAE resistant epoxy to prevent possible outgassing. The epoxy had to have a sufficiently low surface and volume resistivity to prevent charging effects. We found that most epoxies reduce their resistivity by almost two orders of magnitude if the temperature is increased from 20° to 40°C.[4,7] This has lead to a choice of DP-190 epoxy which gives 10^{12} Ω/sq. at 40°C.

Early R&D showed that the presence of TMAE in the gas increases the wire aging rates by a significant factor - see section 3.5. We have implemented a system of nA-meters to monitor the current far below the capability of a typical commercial power supply.[4,8] If the SLC background exceeds a certain limit, causing a current 6 nA per detector, the high voltage is automatically reduced to 80%. This limits accumulation of large charge doses. In principle, such a system could also avoid damage due to Malter currents.[9] One detector developed such a current after ~2 years exposure to TMAE in the 1992 run. The current was observed only in the presence of gating (when gating is on, the positive ions travel toward the gating wire plane[4]). When TMAE was removed from the gas the problem went away. The Malter effect is a particular problem for the "CRID type" of detector operating with TMAE, because unlike all other wire detectors, we cannot add any substantial amount of water or alcohol to our gas (for example, the SLD drift chamber has 0.4% water in the gas mixture). TMAE becomes highly resistive as its purity is increased.

Since 1991 we have broken several 7 μm carbon wires and, of course, this has caused concern. On the other hand, the use of high resistance wire (~40 kΩ/10 cm) makes the chamber very stable, because the wire acts as an impedance in the initial spark formation.

3.2. Design of the single electron detector.

Fig.3a shows the design of the single electron detector. It is based on single stage wire amplification. To prevent the avalanche photons from entering the TPC drift volume, a system of Cu-Be blinds was constructed.[4] To have a good electron transmission to the anode wire, we run a ratio between the drift field within the detector and the drift field in the TPC of close to 6. This makes the structure relatively insensitive to misalignments.[10] For the CRID detector condition, UV photons are created by three carbon excitations[11] - see Fig.3b. The measured rate of afterpulses per avalanche caused by the secondary avalanche photons is less than 1% at our operating point.[4] It depends on the total avalanche charge and not on the electric field near the wire.[4] The Cu-Be blind structure gives us a factor of 7-8 reduction in the rate of the afterpulses - see Fig.3c. Although we block the avalanche photons efficiently with our blinds and prevent them from reaching the active drift volume, they are still generated and can reach the cathode surfaces to create photoelectrons (it takes 10 cm of gas to absorb the C*-1561 A^{o} line). This could contribute to the detector instability, if $\eta G > 1$ (η is ratio of photo-electrons per avalanche electron and G is the wire gain).[12] The fact that the system of 3720 anode wires has been stable for more than 2 years of TMAE operation proves that our design and its operating point are sound.

3.3. Charge division performance.

One needs to measure the y-coordinate along the depth of the drift box to limit the broadening of the photon detection resolution - see Fig.4a. In our case we use charge division to determine this depth. Figs.4b,c show the effect of including charge division on the Cherenkov rings using cosmic rays at SLD. From Figs.4d,e we conclude that the correction for the depth coordinate gives us an improvement in the Cherenkov angle resolution of about 40%.

Fig.5 shows a schematic model of the variables involved in the charge division measurement. The charge division resolution can be calculated from the following formula[13]:

$$\left(\frac{\sigma_z}{\ell}\right) \cong \sqrt{\left(\frac{\sigma_J}{Q^{vis}_{L+R}}\right)^2 + \left(\frac{\sigma_{amp}/\sqrt{2}}{Q^{vis}_{L+R}}\right)^2 \left[\left(\frac{R_{wire} + 2R_{contact} + 2r_{amp}}{R_{wire}}\right)^2 + \left(\frac{2z}{\ell}\right)^2\right]} \quad , \quad (1)$$

where

$$\sigma_J = 2.718\sqrt{\frac{kT\tau}{2(R_{wire} + 2R_{contact} + 2r_{amp})}}$$

$$\sigma_{amp} \cong 2.718\sqrt{\frac{kTR_{eq}(C_{in} + C_{ch})^2}{2\tau}} \quad .$$

In eq.(1), k is the Boltzmann constant; T is absolute temperature; τ is the amplifier shaping time (65 ns); R_{eq} is the equivalent noise resistance of the FET

(~50Ω); C_{in} is the amplifier input capacitance (~10 pf); C_{ch} is the detector capacitance (~15 pf); Q^{vis}_{L+R} is the visible charge (1-2x10^5 el.); $R_{wire} = 41.3 \pm 2.64$ kΩ; $R_{contact} = 94.6 \pm 116\Omega$; and $r_{amp} = 680 \pm 50\Omega$. For typical choices of the amplifier parameters the Johnson noise dominates the problem, so that one needs to use a wire of about 25 kΩ/10 cm of wire length and a gas gain G ~ 2x10^5 to reach 1% resolution. In practice, we had only two choices of wires, the 7 μm carbon wire and the 33 μm carbon wire (R_{wire}~5.2 kΩ/10 cm).[13] Using equation (1), one gets σ_J ~ 960 electrons (with σ_{amp} ~ 530 electrons) for the first wire, and σ_J ~ 2480 electrons for the second wire.[13] R&D tests indicated σ_z/ℓ ~ 0.7% for the first wire, and 1.4% for the second.[4,13] This lead us to choose the 7 μm carbon wire, even though the thinner wire is substantially weaker and more difficult to handle. Unfortunately, the final amplifier layout had worse noise performance (σ_{amp} ~ 1600 electrons), somewhat weakening the argument. Fig.6a shows the R&D test performance with the 7 μm wire. Fig.6b compares the R&D test data with the calculation using the equation (1) - the dashed line shows the calculated results while the solid line is also corrected for the UV gun source width. Fig.6c shows the present SLD performance as obtained using the inclined UV calibration fibers. We get about 2.2 mm for the final resolution after subtracting 1 mm in quadrature due to the source width. The resolution is indeed dominated by the electronics noise (~1.7 mm).[14] If it were not for the wire aging we could increase the wire gain slightly and obtain better results. Other contributors to the charge division resolution are the amplifier gain calibration, amplifier input impedance variation, contact resistance to the carbon wire,[13,15] wire nonuniformity, and wire gain variations.

The overall noise performance of the whole system at SLD is about 2000 electrons. At this noise level a 33 μm carbon wire would provide almost the same resolution. The 33 μm wire would also allow a larger decoupling cathode capacitor resulting in about half the cross-talk.[16]

3.4. Electronics performance.

Since the CRID electronics has a number of novel features compared to other detectors,[17] it is worthwhile discussing a few points in detail. We placed the amplifiers, analog storage, ADC's and a control and multiplexing circuitry on the detector. Only a few serial optical fibers lead to the Fastbus located in the electronics control room. Fig.7 shows the amplifier design. It is based on JFETs and Plessey 3703 semicustom chips. To simplify the deconvolution analysis,[18] it uses RC-CR timing resulting in an exponential pulse waveform response with a shaping time of 65 ns. The amplifier charge gain is about 2.7 μV /electron. To limit the heating problems, all components use pulsed power except the first JFET. The analog storage (HAMU) needs to be calibrated every few days; the amplifier gain is calibrated once per run. The essential requirement of a charge division system is the ability to perform amplifier gain calibrations accurately. Equation (2) shows the variables in the problem (g_i are the amplifier gains).

$$y = \frac{g_1 Q_1 - g_2 Q_2}{g_1 Q_1 + g_2 Q_2} \frac{R_{wire} + 2(r_{amp} + R_{contact})}{R_{wire}} \frac{\ell}{2} \qquad (2)$$

To be able to determine the g_i constants accurately, we actively laser trimmed the resistor in the calibration circuit (R90 in Fig.7) to equalize the response of the amplifier to calibration circuit and the real inputs to 1%.

Equation (3) describes the shape of the single electron pulses by convoluting the amplifier response and the positive ion response[13,19] :

$$C(t) = \int_0^t [t' \exp(\frac{-t'}{\tau})](\frac{1}{t - t' + t_0})dt' = \exp(-\frac{t + t_0}{\tau})(t + t_0)$$
$$x\{\ln(1 + \frac{t}{t_0}) + \sum_{n=1}^{\infty} (\frac{t_0}{\tau}) \frac{1}{n \cdot n!}[(1 + \frac{t}{t_0})^n - 1]\} - \tau[1 - \exp(-\frac{t}{\tau})] \qquad (3)$$

The data agree very well with equation (3) (with $t_0 = 0.1$ ns) as one can see in Fig.8, which shows the results of an R&D test done with CH4 gas and a 7 μm diameter anode wire.

The amplifier-detector combination has cross-talk at a level of +1.1% in the first neighbor and about -0.25% for a distant neighbor.[18] This may seem small, but a typical charged track deposits about 1000 electrons in the TPC so that the cross-talk problem becomes significant. The amplifier response is complicated for very large pulses. Fig.9a shows the amplifier response to a charge of about $3x10^7$ electrons. The amplifier recovery to such charges creates spurious pulses and also affects the measurement of real pulses as one can see in Fig.9b. This is a major complication to the CRID analysis in the core of jets where many tracks overlap. We are still working on various cleaning algorithms.

The ability of our electronics to measure the pulse waveforms has many advantages. Fig.10 shows a complicated event involving a spiraling electron. Such analysis would probably have been impossible with conventional digital electronics.

3.5. Wire aging.

Since the complete waveforms are recorded, wire aging can be studied by monitoring the average single electron pulse height using the UV fibers. Fig.11a shows results of our R&D tests.[20] The TMAE molecule[21] is very susceptible to polymerization because of its double bond structure between carbons and the relative fragility of its other constituents. The prediction from the R&D tests was that a modest detector current of about 5-10 nA would cause a 50% gain drop in about 1-2 years. Fig.11b shows the wire aging at SLD indicating about a 15% gain drop in two years, a result consistent with the R&D data (a typical current 2-4 nA per detector).

To regenerate the wire gain we have shown in R&D tests that we can either wash the detectors with alcohol[20,22] or evaporate the deposits by heating the carbon wires.[16] Because of this problem, we run the detectors at as low a wire gain as possible (average gain at 1-2x10^5), which worsens the charge division performance slightly.

3.6. Distortions due to positive ions.

Fig.12a shows a schematic of the R&D test setup with a laser to measure the distortions induced by positive ions created by a UV lamp.[23] Figs.12b,c show distortions due to the attraction of the drifting electrons by the positive ions located uniformly throughout the TPC volume for two values of the ion concentrations. Fig.12d shows that gating can eliminate the distortions by preventing the positive ions from entering the TPC volume. In the SLD, we monitor this type of distortion by observing the x-coordinate of the UV fiber located at a side of the TPC - see Fig.12e. Fig.12f indicates that we have not seen any change in the distortions due to positive ions at a level of 1 mm during the last run.

3.7. Distortions due to the radial magnetic field component B_r.

Fig.13 shows the measured mean positions of UV fiber hits together with the expected position (solid line) in the x-y plane. Fig.13a shows the pattern of the UV fibers located near the detector for the magnet being off. This and other similar studies[4,23,24] indicate that the distortions for field off are at a level of 1-2 mm at worst. Fig.13b shows the same pattern from UV fibers located at the high voltage end of the TPC with the magnet on. The measured positions of the fibers have clearly shifted from the expected field off positions. To understand this, we calculate the distortion for the B_r component of the magnetic field using the following method. We start with a general equation describing the drift velocity :

$$\vec{v} = \frac{\mu}{1+(\omega\tau)^2}[\vec{E} + \frac{\omega\tau}{B}[\vec{E}\times\vec{B}] + (\omega\tau)^2\frac{\vec{E}\cdot\vec{B}}{B^2}\vec{B}] \qquad (4)$$

We assume the following initial conditions :

$$\vec{B}(0,B_r,B_z), \vec{E}(0,0,E_z), B = |\vec{B}| \approx B_z, B_r(r,z) = B_r^0\frac{rz}{r_0 z_0}.$$

After appropriate integration we obtain the following corrections :

$$\Delta y = \frac{(\omega\tau)^2}{1+(\omega\tau)^2} K r (z_1^2 - z_0^2)$$

$$\Delta x = \frac{\omega\tau}{1+(\omega\tau)^2} K r (z_1^2 - z_0^2) \quad , \qquad (5)$$

where z_1 is the fiber z-position at the high voltage end; z_0 is the z-position of the entrance to the detector; μ is electron mobility; ω is the Larmor frequency; τ is the mean time between collisions; K is a constant; and the result is $\Delta x \sim 9.9$ mm and $\Delta y \sim 8.6$ mm. If one makes the B_r correction using equations (5), one gets good agreement between the reconstructed and expected position of the UV fibers - see Fig.13c. (on the north side it was necessary to introduce an additional systematic correction by rotating all detectors by a few mm about the beam line).

3.8. TPC gas purity.

The C_2H_6 gas is cleaned in the standard way,[25] i.e., we use mechanical filters, Oxisorbs[26] and 13X molecular sieves[27]. In addition, we use electropolished stainless steel tubing as is common practice in Silicon Valley industry. However, U.S. suppliers of ethane have sulfur contamination problems. The sulfur impurity level varies depending on which oil well is used. As much as 200 ppm of sulfur has been reported. The sulfur can exist in ethane as elemental sulfur, CS_2, H_2S, SO_2 and COS. Our initial ethane supply was contaminated at a level of only 1-3 ppm, but that was enough to completely plug up the pressure regulator after one year of operation. We are now using a nickel getter[28] to remove this contaminant. It is delivered with CO_2 to stabilize it. It is then purged with hydrogen gas at elevated temperature to remove the CO_2 in order to activate the nickel. Fig.14a shows that the drift velocity dropped when the nickel cartridge was introduced into the system. This may be explained by the presence of only 0.25% of CO_2 in the ethane gas[29]. One can also see day-to-night variations in the drift velocity. There was also a small release of oxygen over a period of time prompting us to introduce another Oxisorb cartridge. Nevertheless, as one can see in Fig.14b, we did achieve our goal precision for the drift velocity of less than 0.1%. This experience illustrates that some very active substances used in modern cleaning filters can give rise to very complicated chemistry. One possible solution for this particular problem is to buy sulfur-free ethane in Europe.

The TMAE is cleaned by the CRID group by (a) washing it with deionized water, (b) filtering through silica gel and 3A and 5A molecular sieves, and (c) pumping[32] it at about 20 Torr for 2-6 hours. This operation resulted in a reproducible production of good quality TMAE by removing various contaminants, including TMO, which is soluble in water (it has 40x times higher electron capture rates compared to oxygen[30]). Before the TMAE is used in the TPC's, it is "certified" in a small ionization chamber.[31] During the run we rely primarily on the self-monitoring of each TPC by measuring an average TPC z-coordinate formed from single electron pulses and plotting it as a function of time.

Fig.15 shows the photon absorption length in TMAE as measured by various people. Our measurements, using both gas rings and a UV lamp, agree with data of Anderson,[32] perhaps because everyone integrates over the peak in the absorption coefficient at 1900 A°.

3.9. Gas radiator purity.

Our gas radiator recirculation system operates as a heat engine. This was not originally intended, but it was realized that this technique stabilizes the purity. The returning gas mix from the vessel enters a -80°C tank where the C_5F_{12} liquefies and the N_2 gas is vented (requiring about 1 kW in cooling power). The C_5F_{12} liquid is then evaporated again and mixed with the N_2 gas. The overall flow is one complete change every 10-11 hours. In parallel, the C_5F_{12} liquid is circulated through a system of silica gel[33], elemental copper[34], and Oxisorb filters. The logic is that the silica gel protects the other filters[35]. We do not regenerate any of these cartridges because of the fear of the possible dissociation of freon molecules during the heating process. We still have the original 1993 set of cartridges in place 5 months after the start of the 1993 run. Fig.16 shows the UV transmission of a sample taken from the -80°C tank during the run (solid line). The dashed curve indicates the transmission of a sample taken after the tank warmed up at the end of the 1992 run. A subsequent analysis of this sample by the 3M company indicated 84.3% C_5F_{12}, 11.6% C_6F_{14}, 1.01% C_7F_{16}, 1.87% C_8F_{18}, and 1.22% of some other fluorocarbon. Our tests indicate that neither C_7F_{16} nor C_8F_{18} are responsible for the loss of transmission. Therefore, it is the unknown fluorocarbons or other trace components which are likely to be responsible for the loss of transmission. During a run, C_8F_{18} and heavier liquids are frozen in the -80°C tank and kept there until it is warmed up at the end of the run. Similarly, at the end of the run we have found a heavy fluorocarbon (possibly $C_{17}F_{30}$) at the bottom of the evaporator. Therefore, we believe that the simple distillation and freezing cycle in our heat engine recirculation system helps to maintain the required purity of the radiator gas.

Our typical oxygen level in the vessel is 5 ppm and the water level is 40-50 ppm. The gas radiator mixture is continuously monitored by sonar.[35]

3.10. Liquid radiator purity.

Fig.17a,b shows our liquid radiator purity during the run. The dashed curve indicates what happens if we stop the recirculation for a long time period. The liquid is initially de-oxygenated and purified by bubbling N_2 gas through it. During the run, the liquid is purified by pumping it through an Oxisorb cartridge. The recirculation flow is one radiator volume every 2 hours. The Oxisorb is changed every 3 months. In this system the Oxisorb is not protected by silica gel. In view of recent findings in the DELPHI group,[37] perhaps this could be a mistake in the long run. However, we do know that 3M Co. uses silica gel to clean the liquid before shipping, and our experience to date is satisfactory.

3.11. Approximate estimate of N_o.

Fig.18 shows some components of the efficiency for the transport and the conversion process into photoelectrons. They are derived from a collection of efficiencies either measured during the construction period (transmission of quartz, mirror reflectivity and TMAE quantum efficiency[11,38]), efficiencies measured during the run (UV transmission of fluorocarbons, oxygen and water effects), and estimates for other factors such as absorption by the field cage wires, chamber efficiencies, and electron lifetime. The resulting final efficiency is shown by the open circles in Fig.18, and is then integrated as a function of wavelength to estimate N_o. The final estimated N_o is 56-66 cm^{-1} for the gas rings and 32-42 cm^{-1} for the liquid rings (if the gaps between TPC's are not taken into account the latter number increases to 45-55 cm^{-1}). The range of estimated N_o depends on the assumptions, such as, for example, what TMAE quantum efficiency is used[11,38]. This method does not include effects such as confusion in the middle of jets (and small electron losses due to the Lorentz angle in the liquid rings). Therefore, it is expected to be most useful for simple events, such as cosmic rays, di-muons, Bhabhas, etc. Such data appear to support more optimistic values for N_o. For example, for the cosmic rays we observe : 17-18 photo-electrons per full liquid ring, and ~8 per gas ring, which implies $N_o = 45$ cm^{-1} for liquid and 63 cm^{-1} for gas.

4. RESULTS AT SLD

Fig.19 shows liquid rings from hadronic Z_o events. The present background situation can be understood from Fig.20, where we show the effect of removing different background hits : (a) corresponds to all photoelectron hit candidates; (b) also includes removing hits with a long TMAE absorption length; and (c) includes the cross-talk and amplifier recovery cleaning cuts. One can see that the last cut removes a significant amount of background, but also removes signal hits. It is still being refined. The local Cherenkov angle resolution per photon is about 12 mrad, close to the design value; however, we still have about 10 mrad of systematic errors due to various global misalignments. Fig.21 shows the first attempt at particle identification using fitted liquid rings.

Fig.22 shows gas rings in the hadronic Z_0 events. We get about 7-8 photoelectrons per ring, and the local resolution with respect to the ring is close to the design value of 4-5 mrad (FWHM). Again, we still are dealing with systematic alignment errors at a level of 10 mrad.

5. WHAT DID WE LEARN ?

One can summarize briefly what we have learned during the CRID development (For the benefit of newcomers to this field we would like to stress that some items were far from obvious when we started) :

1. Single electron detection on a large scale is possible.
2. Charge division on single electrons works.
3. It is possible to build a 60 kV system without a field degrader.
4. Positive ion distortions during SLD data taking have not yet been seen.
5. TMAE wire aging does indeed exist, and the rate is consistent with R&D results.
6. Glues and materials selected during the R&D phase have behaved as predicted. Long electron lifetimes can be maintained.
7. It is possible to make a large system which is leak tight to less than 1 ppm of oxygen level, which is needed in the TPC's.
8. Fluorocarbons can be cleaned and recirculated.
9. Ethane can have a sulfur contamination; active surfaces of the filters, such as nickel, can introduce complicated chemistry problems.
10. Given the noise performance in a large system, we could have used the 33 μm carbon wire instead of 7 μm carbon wire. It would improve the mechanical integrity of the anode wires.
11. A substantial technical effort is required to keep the system operational for many years.
12. The thick TPC causes very large dE/dx deposits to which the amplifier responds in rather complicated ways; in retrospect, a logarithmic amplifier response might have avoided some of these problems.

13. It takes a large effort to tune the software analysis to obtain even minimal performance in a large 4π CRID detector.

FIGURE CAPTIONS :

1. Schematic of the SLD barrel CRID.
2. Principle of photoelectron detection in the barrel CRID.
3. (a) Geometry of the single electron detector; (b) sensitivity to carbon excitation lines in CRID; (c) rate of afterpulses as a function of total visible charge in the avalanche with and without blinds.
4. Equivalent model of charge division and its variables.
5. (a) Principle of parallax broadening of the image due to depth of the TPC; liquid rings (b) with and (c) without charge division; and resulting Cherenkov angle resolution (d) with and (e) without the charge division information (about 40% worse) .
6. (a) Measured R&D results on charge division resolution in C_2H_6 gas with 7 μm diameter carbon wires at cathode voltage $V_c = -1.55$ kV;[13] (b) Measured R&D results integrated over all pulse heights on a single photoelectron as a function of z-coordinate along the wire on 7 μm (▯) and 33 μm (Δ) wires;[13] calculation done using equation (1) assuming the average visible charge of 2.25×10^5 and 2.5×10^5 electrons for both types of wires (dashed lines include 400 μm beam size); and (c) present SLD measured charge division result on the system of 3700 wires at $V_c = -1.50$ kV (it includes 1 mm contribution from the UV fiber beam size).
7. CRID amplifier circuit including the calibration circuit with the laser trimmed resistor (R90).
8. 11. (a) The average measured single electron pulse shape obtained with 7 μm wires in CH_4 gas;[13] (b) Comparison of an average measured test pulse shape (Δ) and the calculated amplifier response $t\exp(-t/\tau)$ (solid line), and the average single-electron measured pulse shape (▯) and its calculated shape (dashed line) using eq.(3).[13]
9. (a) Response of the amplifier to very large pulses (3×10^7 electrons); and (b) spurious points on the Cherenkov ring due to the amplifier recovery and/or its effect on real pulses.
10. Power of waveform readout utilizing charge division to disentangle complicated events; (a,b) signal from the two wire ends; and (c) reconstructed spiraling track.

11. Measured wire aging rate using 7 μm diameter carbon wires with TMAE during : (a) R&D tests[20] (CRID uses C_2H_6 gas - (Δ) points); and (b) the SLD results (15% gain drop in two years of running).
12. R&D tests : (a) Distortion of a laser track due to positive ions for (b) 0.5×10^6 ions/cm^3; (c) 2.5×10^6 ions/cm^3; (d) as (b), but with the gating on; SLD performance : (e) distortion of UV fiber x-coordinate due to positive ions; (f) its time history (no effect at 1 mm level seen).
13. Measured mean position of UV fibers in the SLD with magnet off : (a) fibers at the detector end; and with the magnet on : (b) before ($\Delta x \sim 9.9$ mm, $\Delta y \sim 8.6$ mm); and (c) after the correction for the B_r effect.
14. (a) Drift velocity in C_2H_6+TMAE measured in the TPC's before and after the introduction of the nickel filter to remove the sulfur contamination (data are consistent with a model[29] that 0.25% of CO_2 is causing the drift velocity drop); (b) a spline fit indicating that the 0.1% precision in the drift velocity monitoring was achieved.
15. Photon absorption in TMAE as a function of the TMAE bubbler temperature from various sources including CRID.
16. Measured UV transmission in 1 cm liquid C_5F_{12} during the CRID operation (solid line), and after the -80°C tank warmed up at the end of run (dashed line).
17. (a) Measured UV transmission in 1 cm liquid C_6F_{14} during CRID operation (solid line), and effect of epoxy outgasing when circulation stopped for many hours (dashed line); and (b) time history of the UV transmission at 1800 A^o indicating the CRID purity stability in the 1993 run.
18. CRID final estimated efficiency (open circles) for (a) gas and (b) liquid rings; several examples of the main efficiency factors also included (TMAE quantum efficiency taken from ref.37, other factors taken from either SLD monitoring or the R&D test data).
19. (a) Full and (b) half liquid rings integrated over many hadronic Z_o events taken by CRID at SLD (all cleaning cuts applied to data).
20. Typical photoelectron background in the liquid rings in the hadronic Z_o events (a) before cuts; (b) after TMAE depth cut; (c) as (b), but also include the electronics cross-talk and recovery cleaning cuts.
21. The first attempts to do particle identification using the liquid rings in hadronic Z_o events by CRID at SLD.

22. (a) Gas rings integrated over many hadronic Z_0 events; (b) ring radius with typical photoelectron background; (c) average number of photoelectrons per ring; and (d) typical local resolution in respect to a ring.

REFERENCES :

[1] J. Sequinot and T. Ypsilantis, Nucl. Instr.&Meth.,142(1977)377.

[2] DELPHI Proposal, LEPC 83-3 and LEPC 84-16,
and U. Ullaland, DELPHI RICH presentation at this conference, Bari, 1993.

[3] D.W.G.S. Leith, Nucl. Instr.&Meth., A265(1988)120.

[4] K. Abe et.al., 5-th International Conference on Instrumentation for Colliding Beam Physics, Novosibirsk, Russia, March 15, 1990.

[5] K. Abe et.al., Nucl.Instr.&Meth., A300(1991)501.

[6] Viton O-ring, Parker Co., Part number : V0747-75, Cure 4Q87.

[7] J.Va'vra, CRID Note#37, Jan.27, 1988.

[8] P. Rensing and J. Va'vra, CRID Note #72, April 1993.

[9] L. Malter, Phys. Rev., 50(1936)48.

[10] D. Aston et.al., IEEE Trans.Nucl.Sci., NS-36,p.276, Feb.1989.

[11] R. Arnold, Y. Giomataris, J.L. Guyonnet, A. Racz, J. Sequinot, and T. Ypsilantis, CERN-LAA/PI/91-014.

[12] P.Fonte, V. Peskov and F. Sauli, Nucl.Instr.&Meth., A305(1991)91.

[13] D. Aston et.al., Nucl.Instr.&Meth., A283(1989)582.

[14] F. Suekane and Y. Iwasaki, CRID Note #79, March 24, 1993.

[15] J. Va'vra, CRID Note #75, Nov.24, 1992.

[16] J. Va'vra et.al., IEEE Trans. Nucl. Sci., NS-35, p.487, Feb.1988.

[17] E. Spencer et.al., IEEE Trans.Nucl.Sci., NS-35,p.231, Feb.1988; P. Antilogus et.al., SLAC-PUB-5120, Oct. 1990; K. Abe et.al., SLAC-PUB-5679, Nov. 1991.

[18] P. Rensing, Ph.D. thesis, SLAC Report 421, Stanford, August 1993.

[19] J. Va'vra, CRID Note #50, August 1988.

[20] J. Va'vra, IEEE Trans. Nucl. Sci., NS-34, p.486, Feb. 1987.

[21] TMAE stands for Tetrakis dimethylamino ethylene and was purchased from RSA Co., U.S.A.

[22] K. Martens et.al., OMEGA RICH presentation at this conference, Bari, 1993.

[23] P. Antilogus et.al., SLAC-PUB-5365, Feb. 1991.

[24] M. Cavalli-Sforza et.al., IEEE Trans. Nucl. Sci., NS-37, p.1132, June1990.

[25] K. Abe et.al., SLAC-PUB-5988, October 1992.

[26] Oxisorb made by Messer Griesheim GmbH, 4000 Dusseldorf, Germany.

[27] 13X Molecular Sieve made by Union Carbide Co., Danburg,CT 06817-0001, U.S.A.

[28] Nickel catalyst N1-0104T-1/8 made by Engelhard Co., Iselin,NJ 08830-0770, U.S.A.

[29] Calculation was performed by S. Biaggi with his Magboltz program.

[30] R.T. Rewick, T. Weber, M. Cavalli-Sforza, M.L. Schumacher, and S. Shapiro, Anal.Chem., 60(1989)2095.

[31] M. Cavalli-Sforza, CRID Note#15, May 1986.

[32] D. Anderson, IEEE Trans. Nucl. Sci., NS-28, p.842, Feb. 1981.

[33] Silica Gel Sorbead R was purchased from Adcoa Co., Gardena, CA 90247, U.S.A.

[34] Elemental Copper is made by Engelhard Co., Elyria, OH 44035, U.S.A.

[35] The procedure recommended to us by 3M Co., St. Paul, Minn. 55144-1000, U.S.A.

[36] G. Hallewell et.al., SLAC-PUB-4405, 1987, and his talk at this conference.

[37] S. Ilie and G. Lenzen, DELPHI 93-33 RICH 54.

[38] R.A. Holroyd, J.M. Preses, C.L. Woody, and R.A. Johnson, Nucl.Instr.&Meth, A261(1987)446.

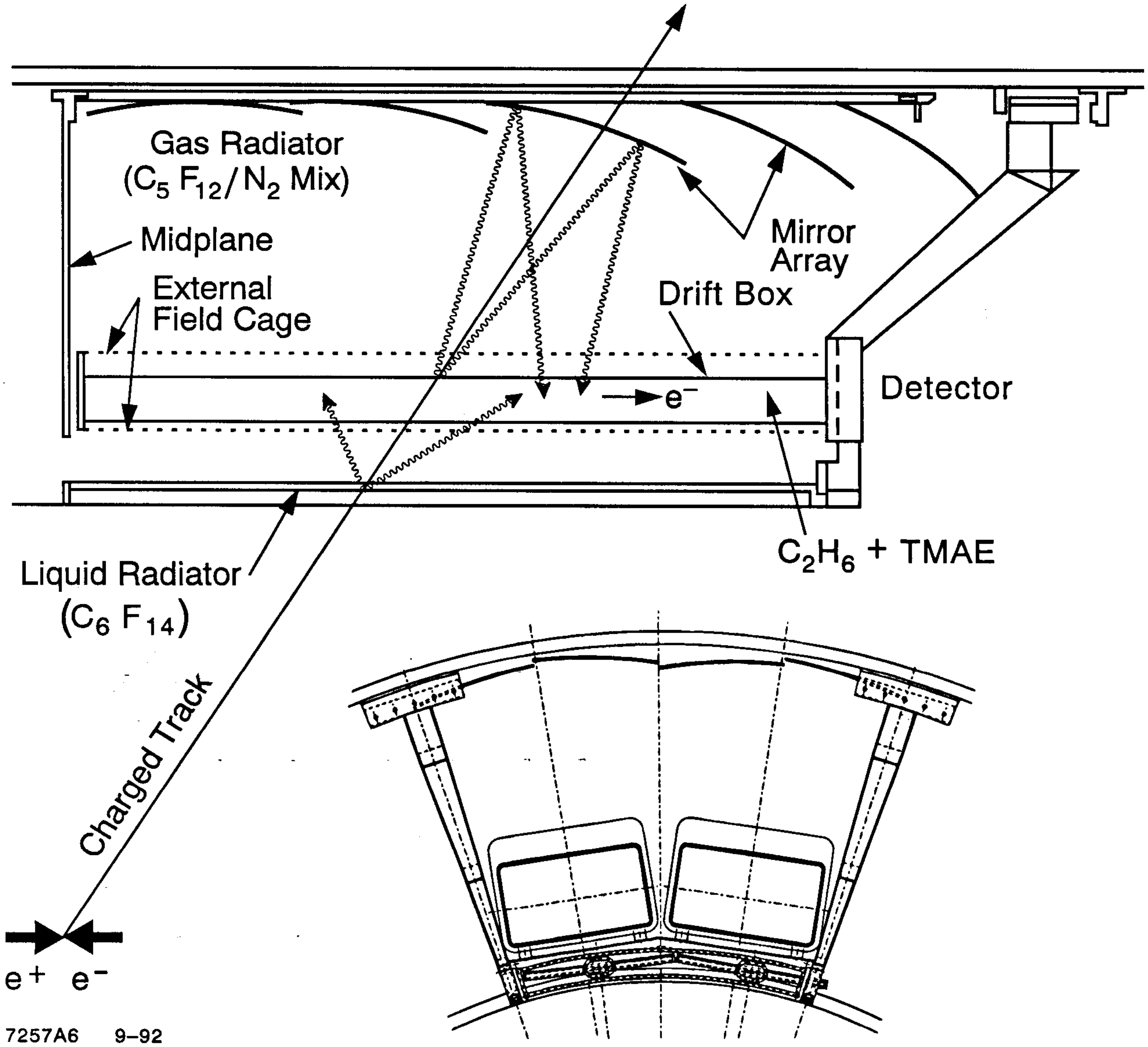
Gas Radiator
(C_5F_{12}/N_2 Mix)
Midplane
External
Field Cage
Mirror
Array
Drift Box
Detector
e^-
C_2H_6 + TMAE
Liquid Radiator
(C_6F_{14})
Charged Track
e^+ e^-
7257A6 9–92

Fig. 1

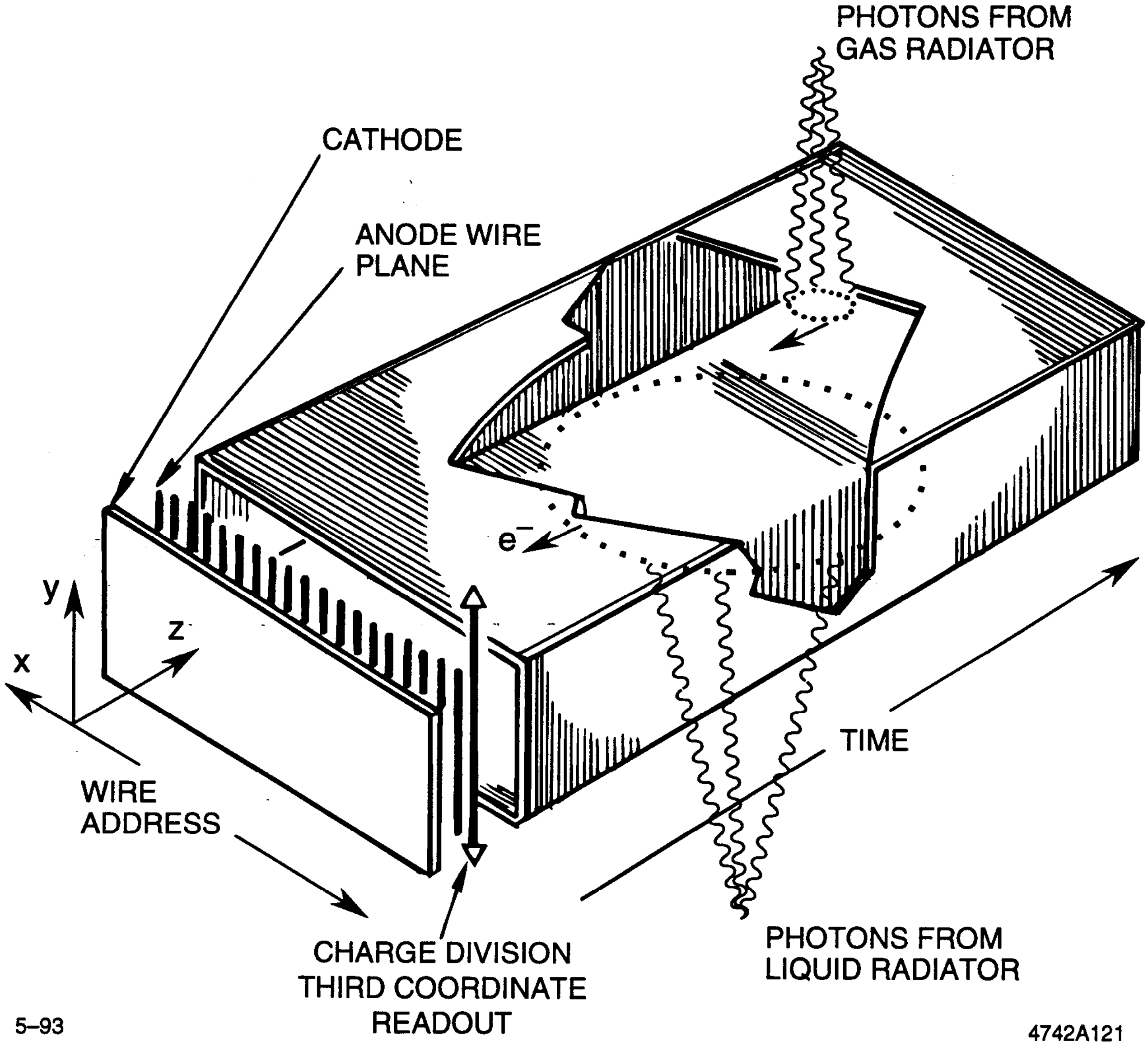
PHOTONS FROM GAS RADIATOR
CATHODE
ANODE WIRE PLANE
e⁻
y
z
x
WIRE ADDRESS
TIME
CHARGE DIVISION THIRD COORDINATE READOUT
PHOTONS FROM LIQUID RADIATOR
5–93
4742A121

Fig. 2

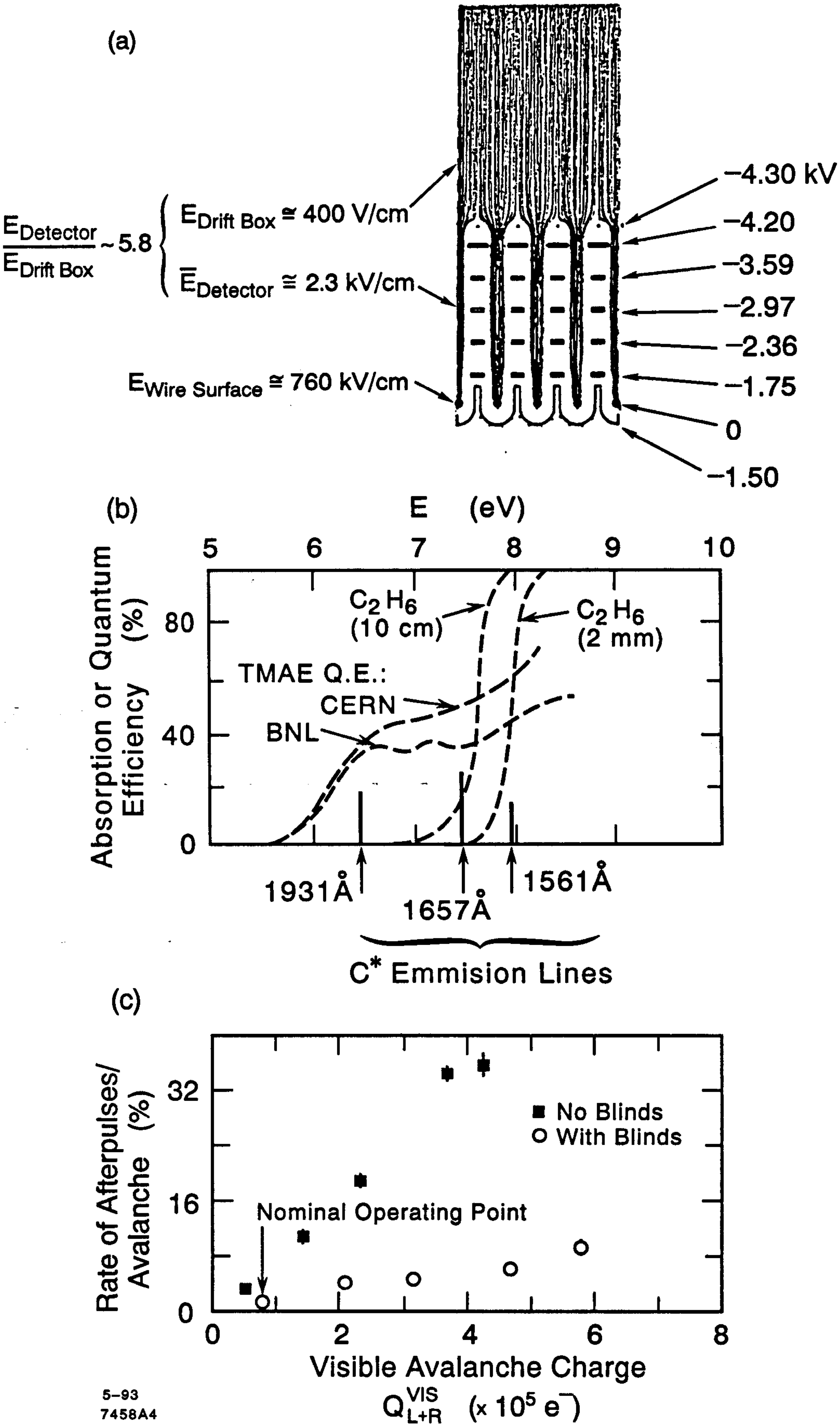
(a)
$E_{Detector}/E_{Drift Box}$ ~ 5.8
$E_{Drift Box}$ ≅ 400 V/cm
$\bar{E}_{Detector}$ ≅ 2.3 kV/cm
$E_{Wire Surface}$ ≅ 760 kV/cm
−4.30 kV
−4.20
−3.59
−2.97
−2.36
−1.75
0
−1.50
(b)
E (eV)
5
6
7
8
9
10
Absorption or Quantum Efficiency (%)
80
40
0
C_2H_6 (10 cm)
C_2H_6 (2 mm)
TMAE Q.E.:
CERN
BNL
1931Å
1657Å
1561Å
C* Emmision Lines
(c)
Rate of Afterpulses/ Avalanche (%)
32
16
0
■ No Blinds
○ With Blinds
Nominal Operating Point
0
2
4
6
8
Visible Avalanche Charge
Q^{VIS}_{L+R} (x 10^5 e^-)
5–93
7458A4

Fig. 3

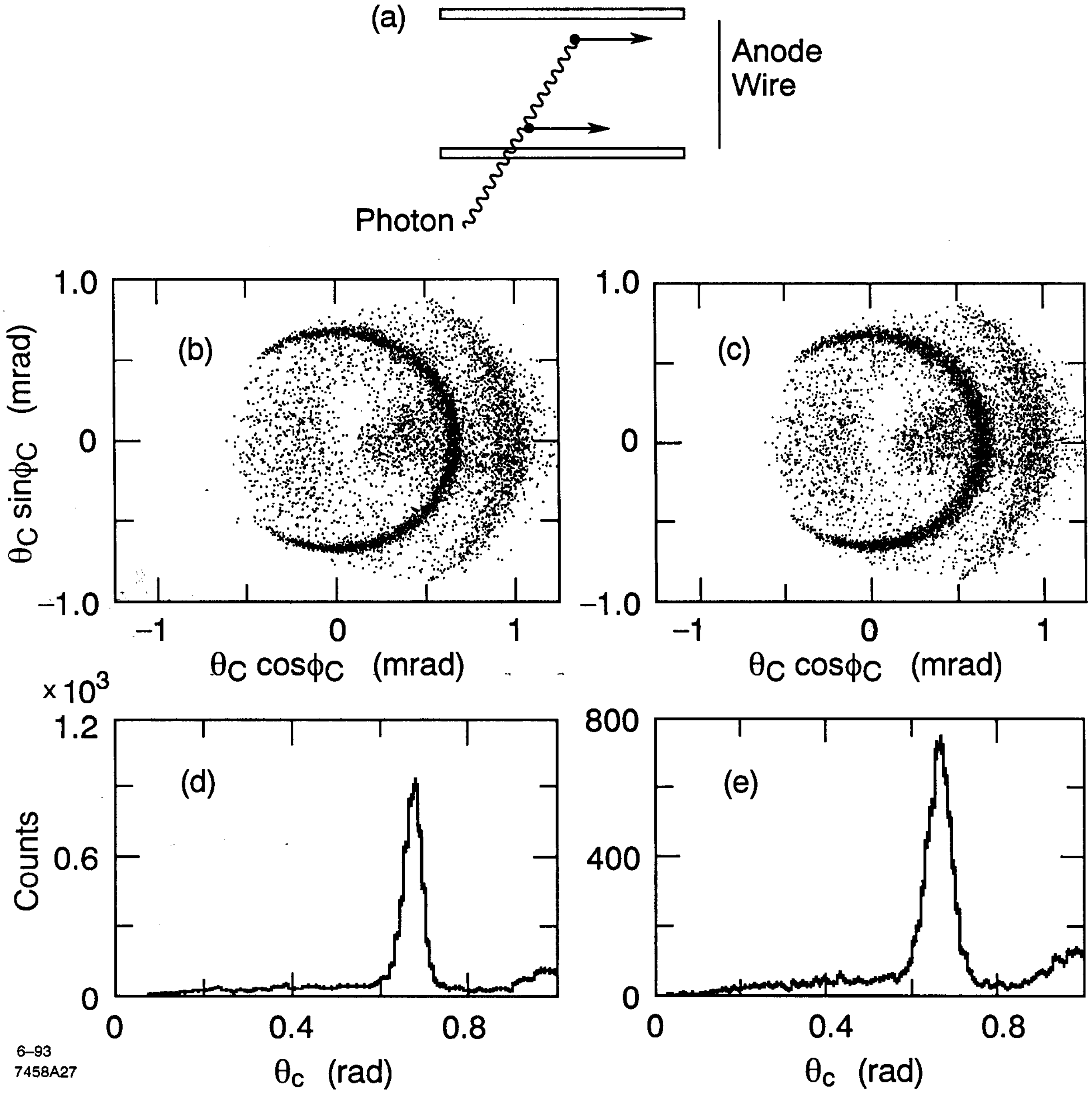
(a)
Anode
Wire
Photon
(b)
(c)
1.0
0
−1.0
−1
0
1
$\theta_C \sin\phi_C$ (mrad)
$\theta_C \cos\phi_C$ (mrad)
(d)
(e)
$\times 10^3$
1.2
0.6
0
800
400
0
0.4
0.8
Counts
θ_c (rad)
6–93
7458A27

Fig. 4

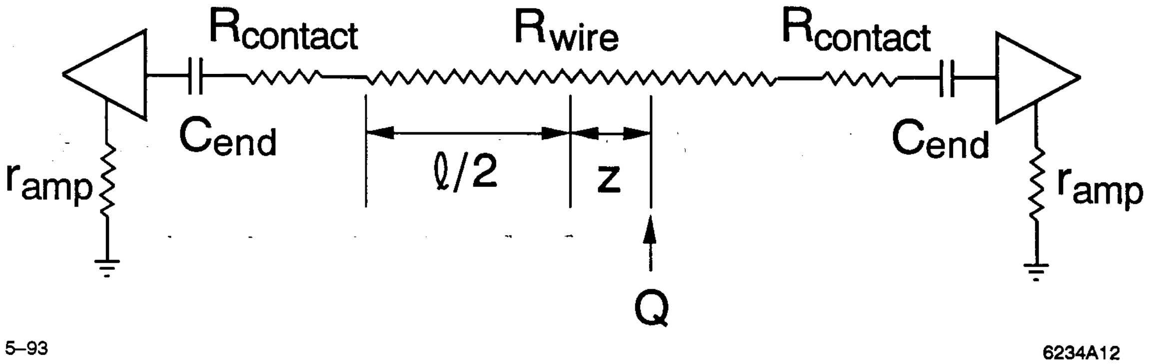

$R_{contact}$
R_{wire}
$R_{contact}$
C_{end}
C_{end}
r_{amp}
r_{amp}
$\ell/2$
z
Q
5–93
6234A12

Fig. 5

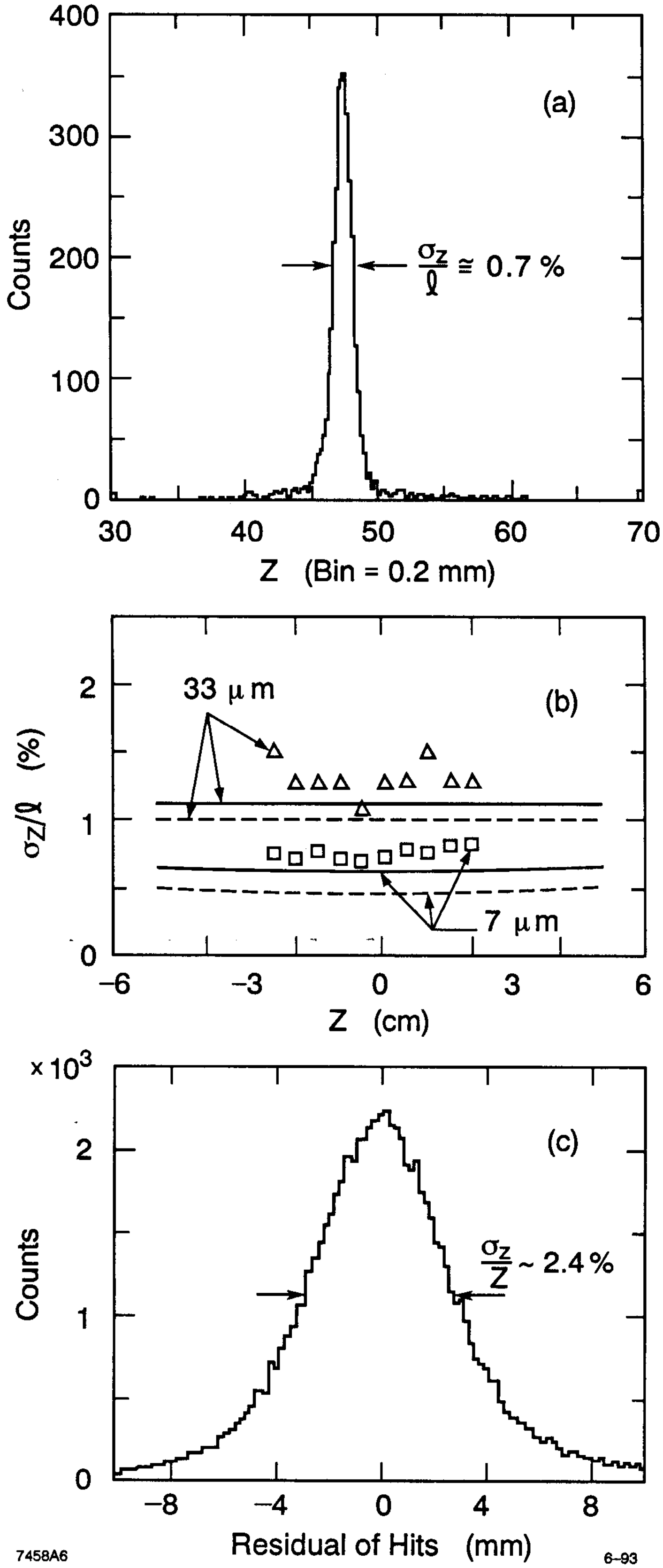
400
300
200
100
0
Counts
(a)
$\frac{\sigma_z}{\ell} \cong 0.7\ \%$
30
40
50
60
70
Z (Bin = 0.2 mm)
2
1
0
σ_Z/ℓ (%)
33 μm
(b)
7 μm
−6
−3
0
3
6
Z (cm)
x 10³
2
1
0
Counts
(c)
$\frac{\sigma_z}{Z} \sim 2.4\ \%$
−8
−4
0
4
8
Residual of Hits (mm)
7458A6
6-93

Fig. 6

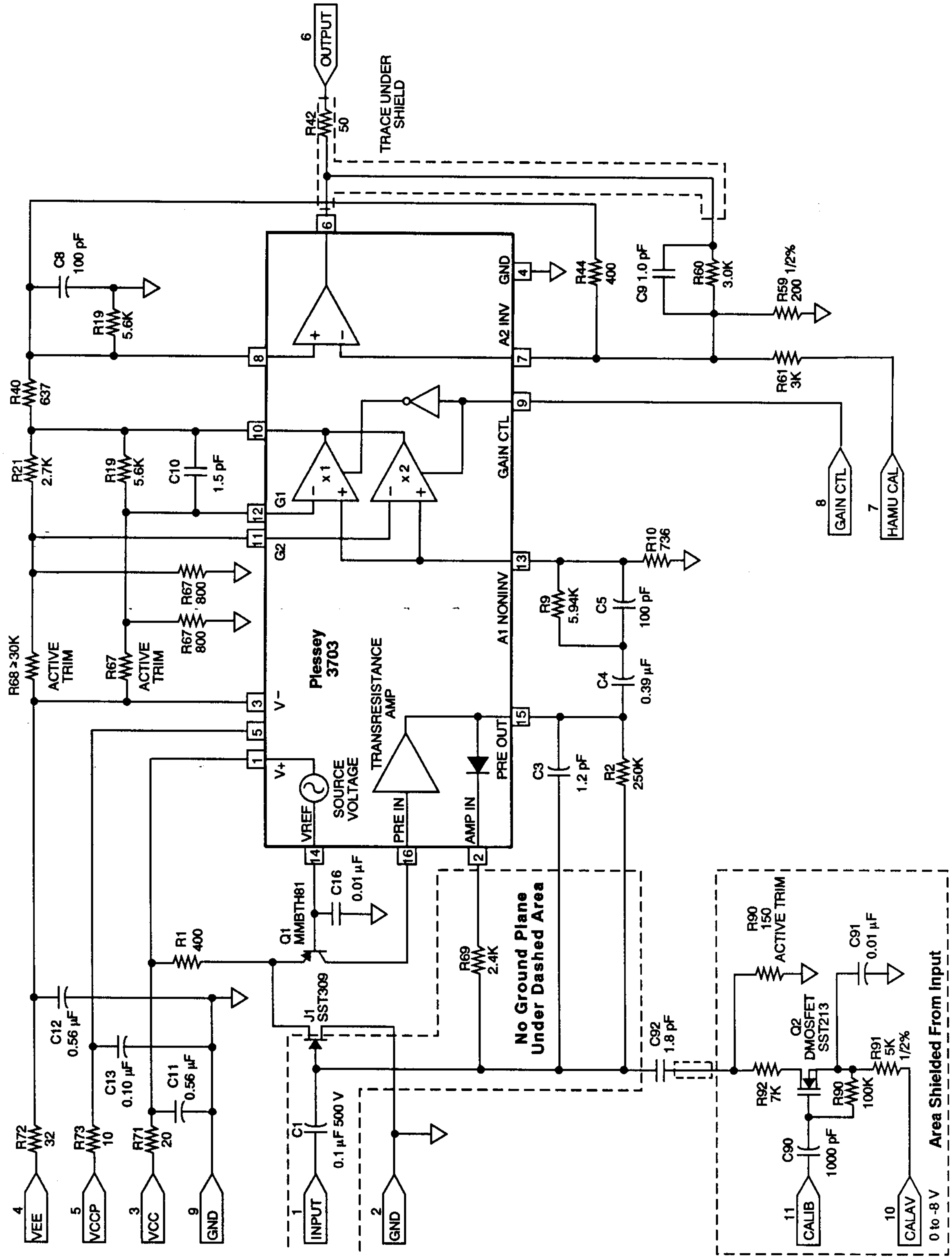

10-89
6489A2

Fig. 7

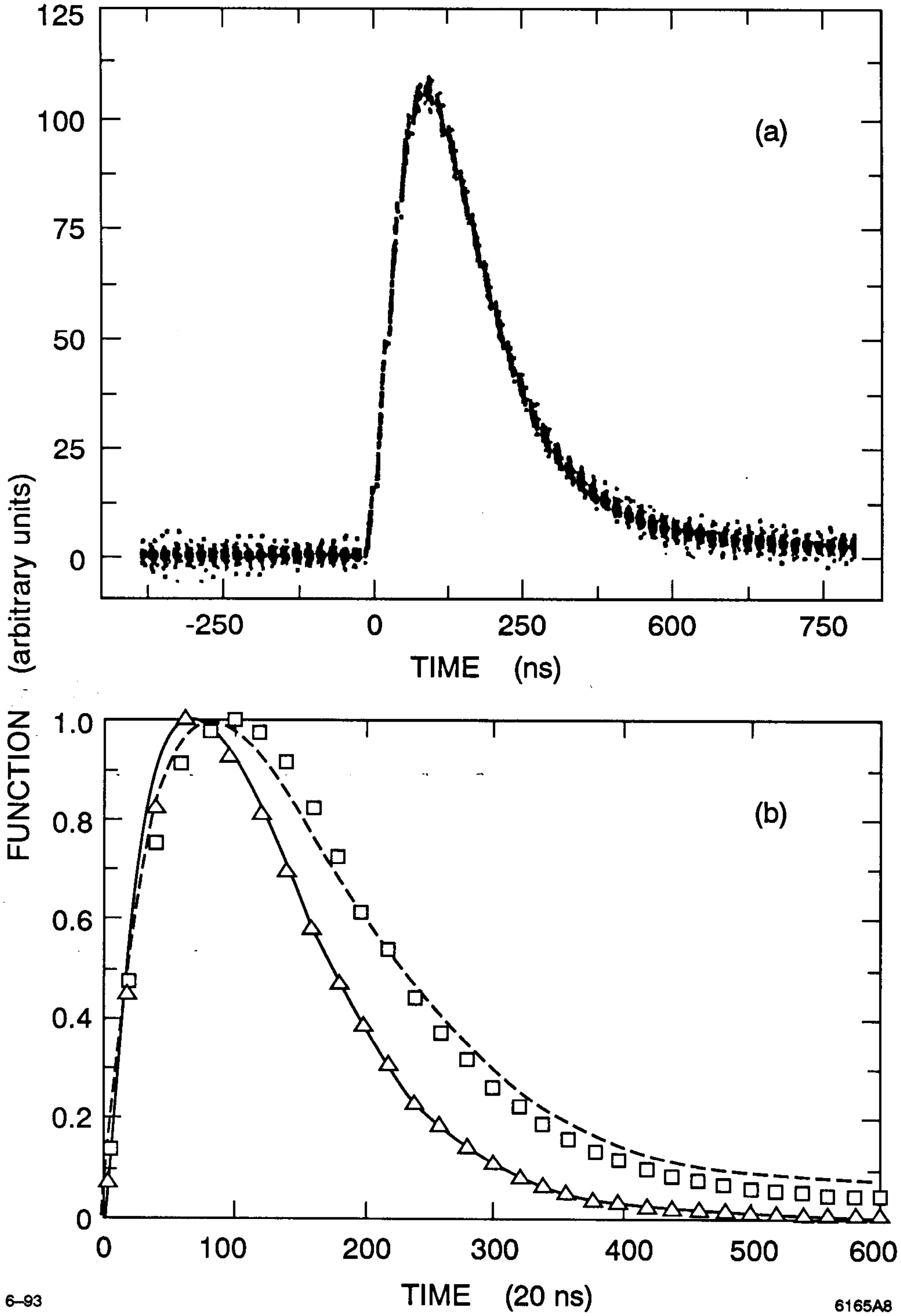
125
100
75
50
25
0
(a)
-250
0
250
600
750
TIME (ns)
FUNCTION (arbitrary units)
1.0
0.8
0.6
0.4
0.2
0
(b)
0
100
200
300
400
500
600
TIME (20 ns)
6–93
6165A8

Fig. 8

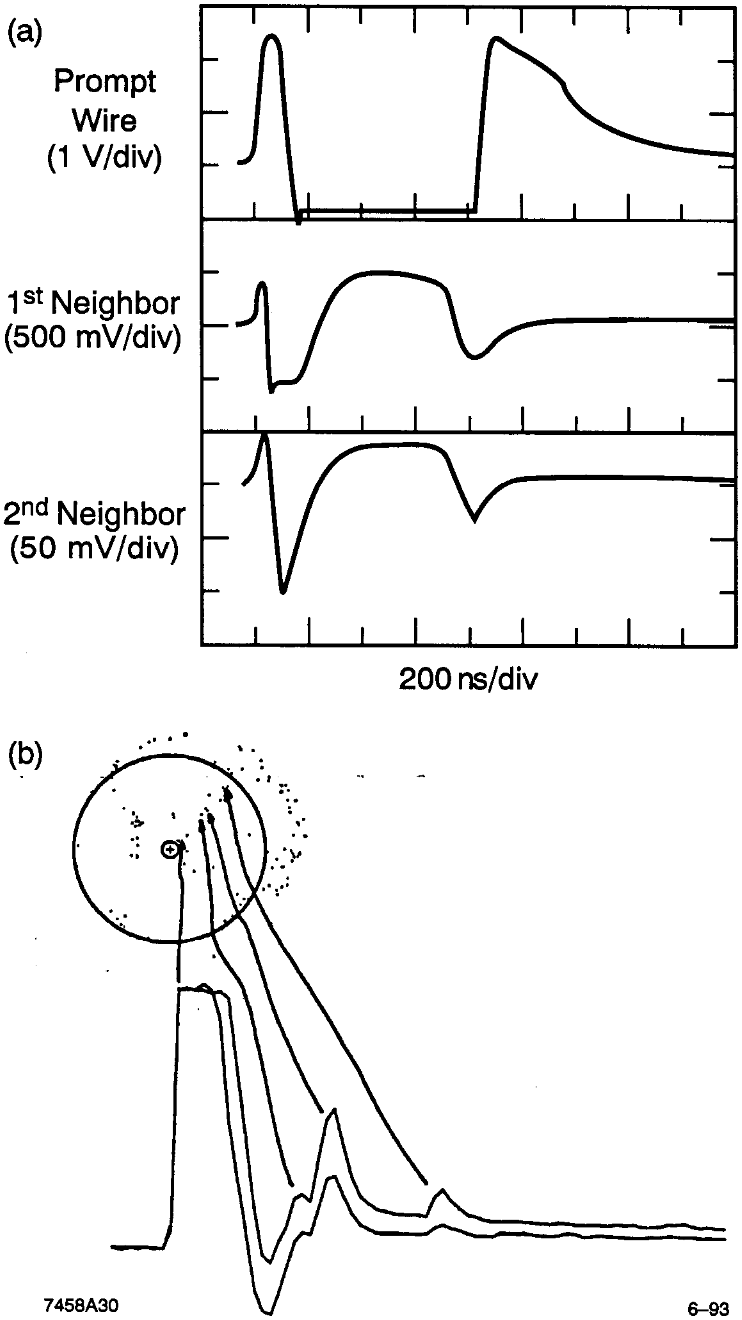
(a)
Prompt Wire (1 V/div)
1st Neighbor (500 mV/div)
2nd Neighbor (50 mV/div)
200 ns/div
(b)
7458A30
6–93

Fig. 9

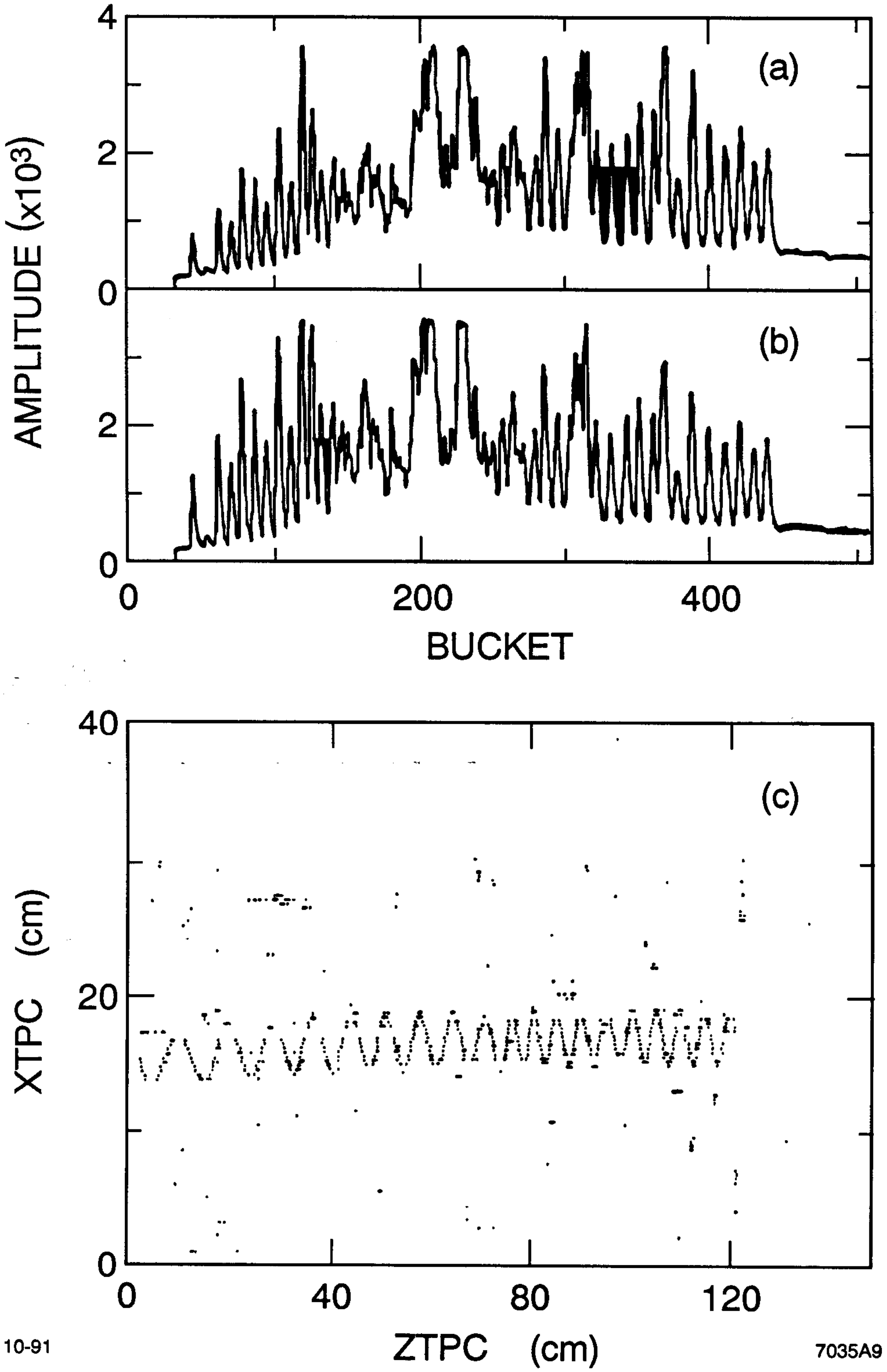
AMPLITUDE (x10³)
4
2
0
2
0
(a)
(b)
0
200
400
BUCKET
40
20
0
(c)
XTPC (cm)
0
40
80
120
ZTPC (cm)
10-91
7035A9

Fig. 10

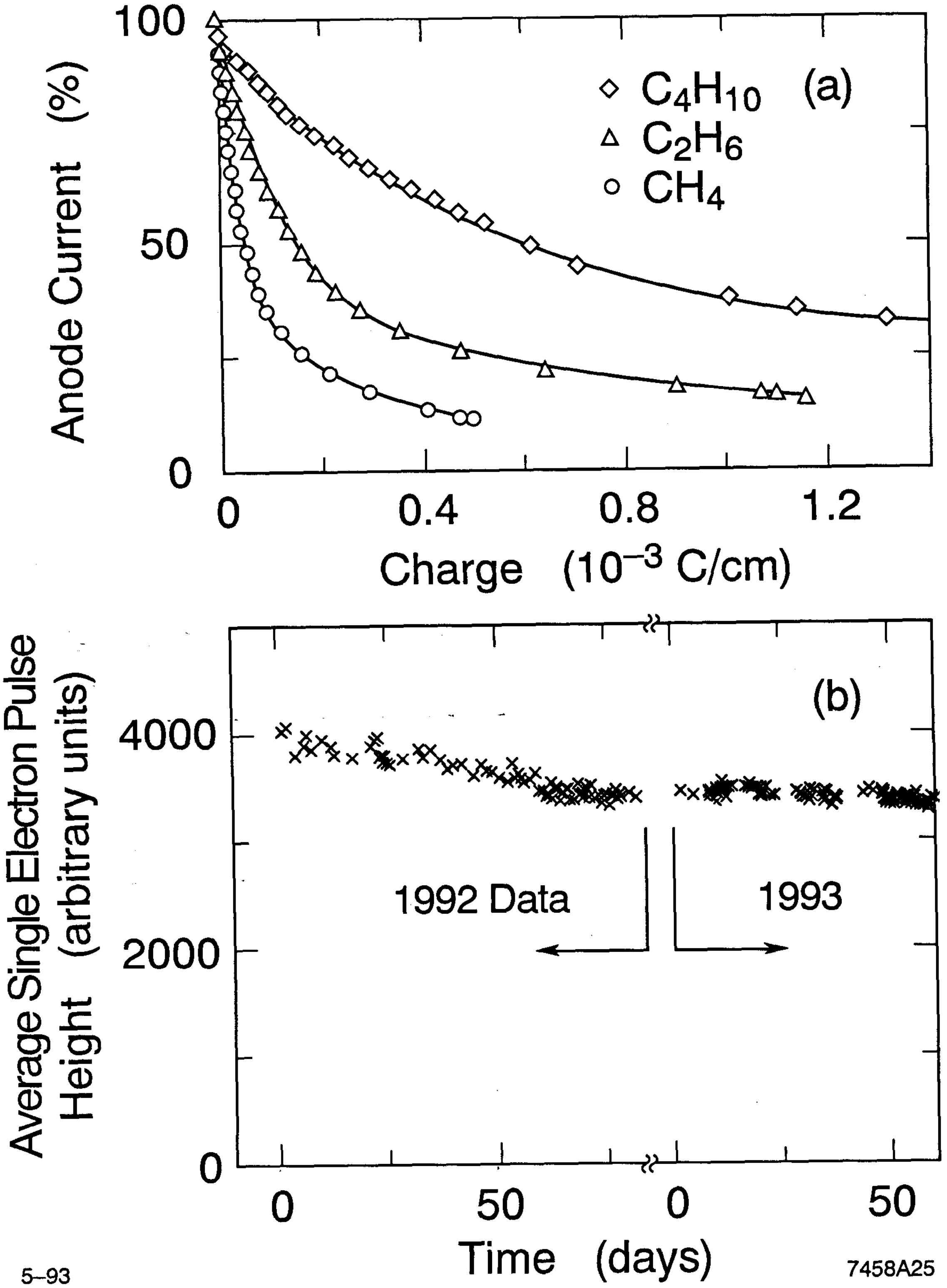
100
50
0
Anode Current (%)
◇ C_4H_{10}
△ C_2H_6
○ CH_4
(a)
0
0.4
0.8
1.2
Charge (10^{-3} C/cm)
4000
2000
0
Average Single Electron Pulse Height (arbitrary units)
(b)
1992 Data
1993
0
50
0
50
Time (days)
5–93
7458A25

Fig. 11

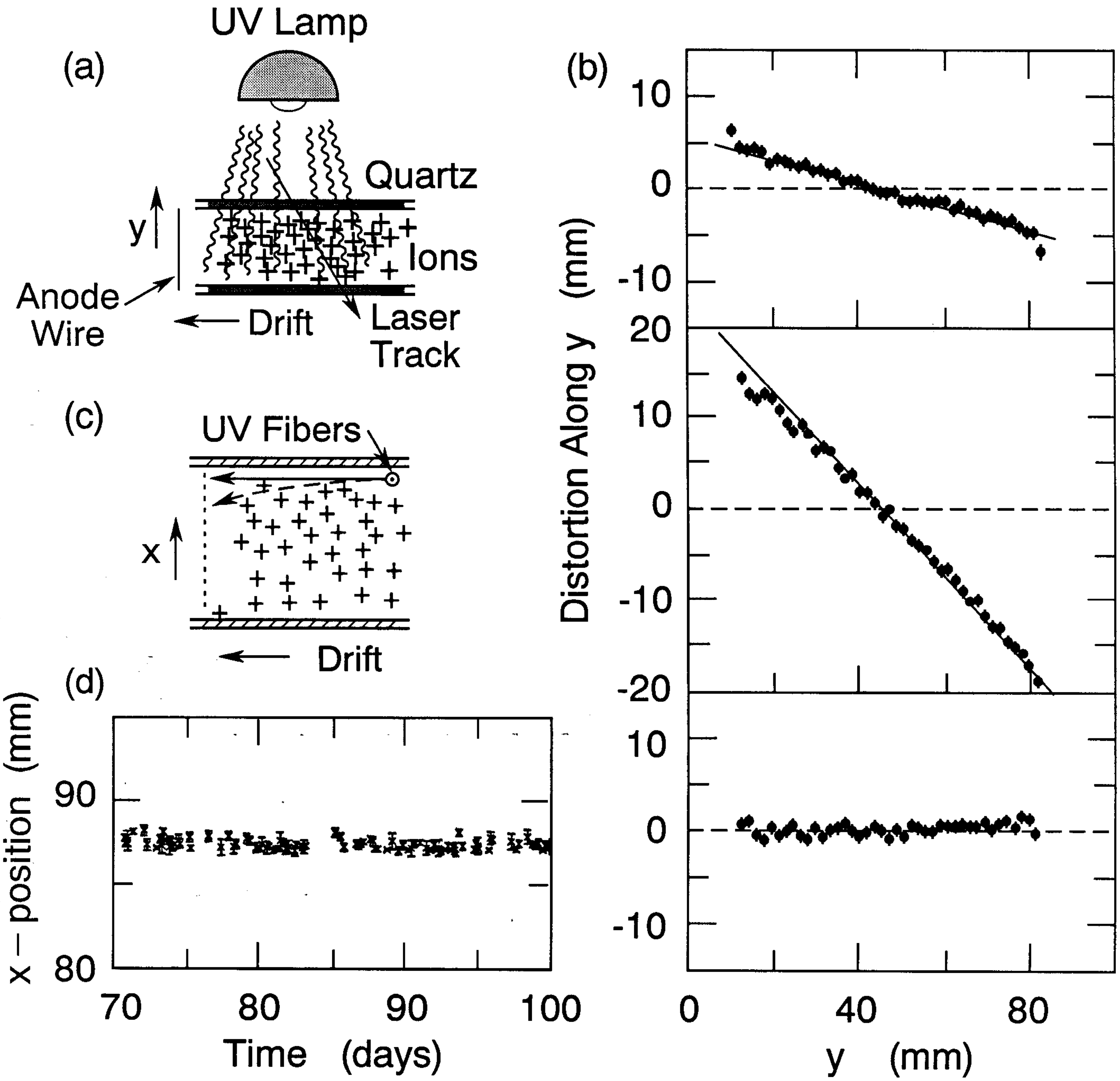

6–93
7458A29

Fig. 12

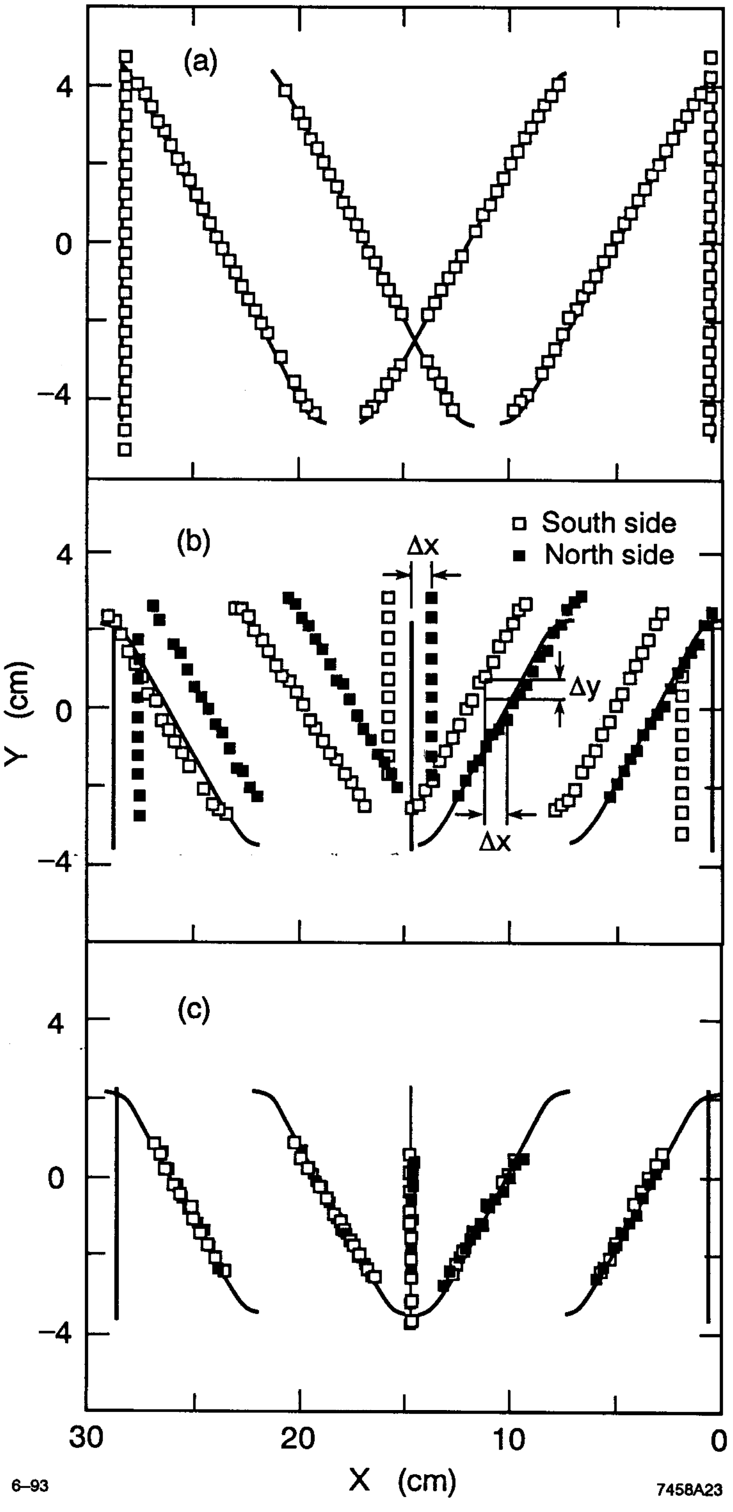
(a)
(b)
(c)
□ South side
■ North side
Δx
Δy
Δx
4
0
−4
Y (cm)
X (cm)
30
20
10
0
6–93
7458A23

Fig. 13

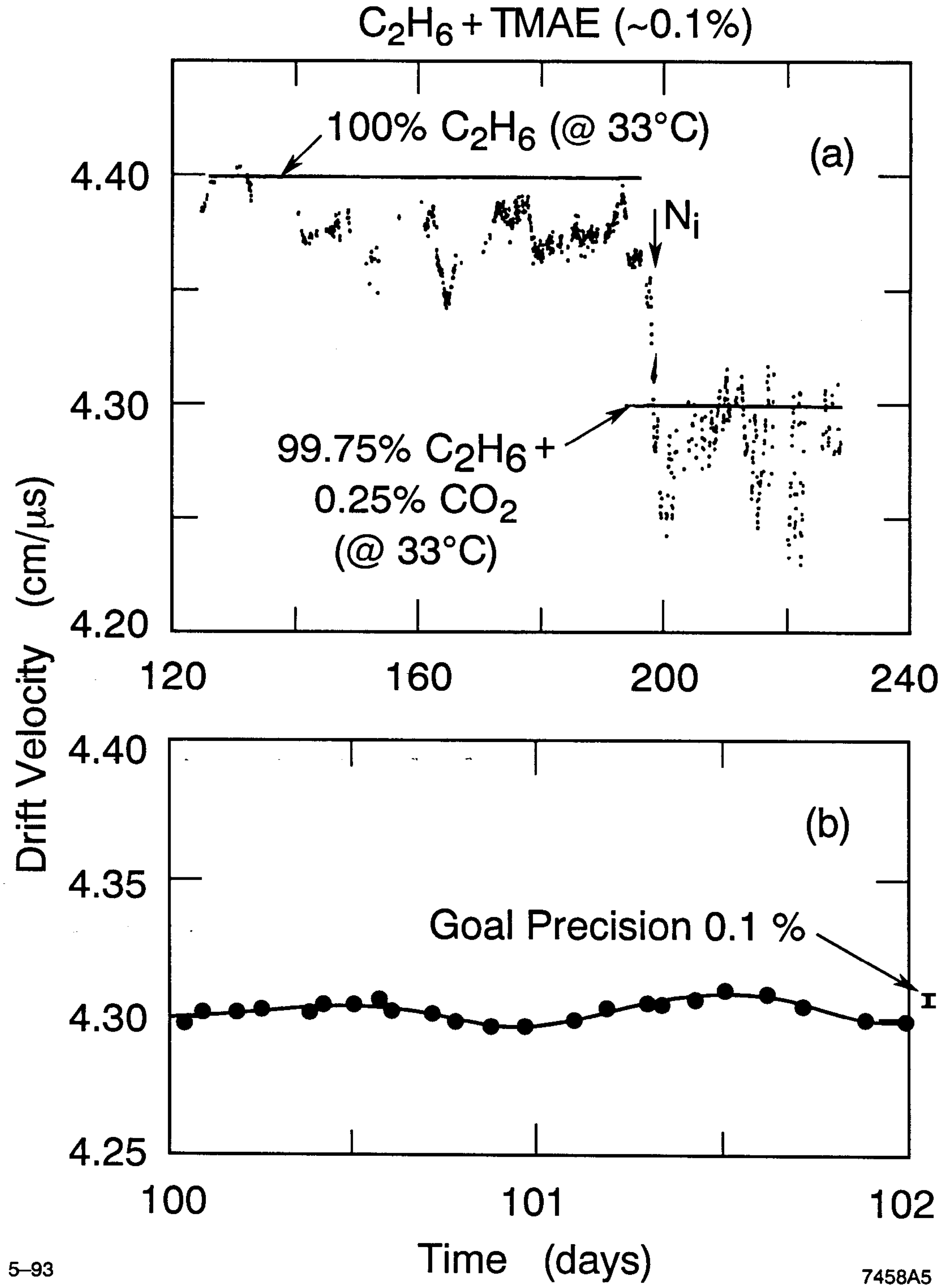

C_2H_6 + TMAE (~0.1%)
100% C_2H_6 (@ 33°C)
(a)
N_i
99.75% C_2H_6 +
0.25% CO_2
(@ 33°C)
4.40
4.30
4.20
120
160
200
240
Drift Velocity (cm/µs)
4.40
4.35
4.30
4.25
(b)
Goal Precision 0.1 %
100
101
102
Time (days)
5–93
7458A5

Fig. 14

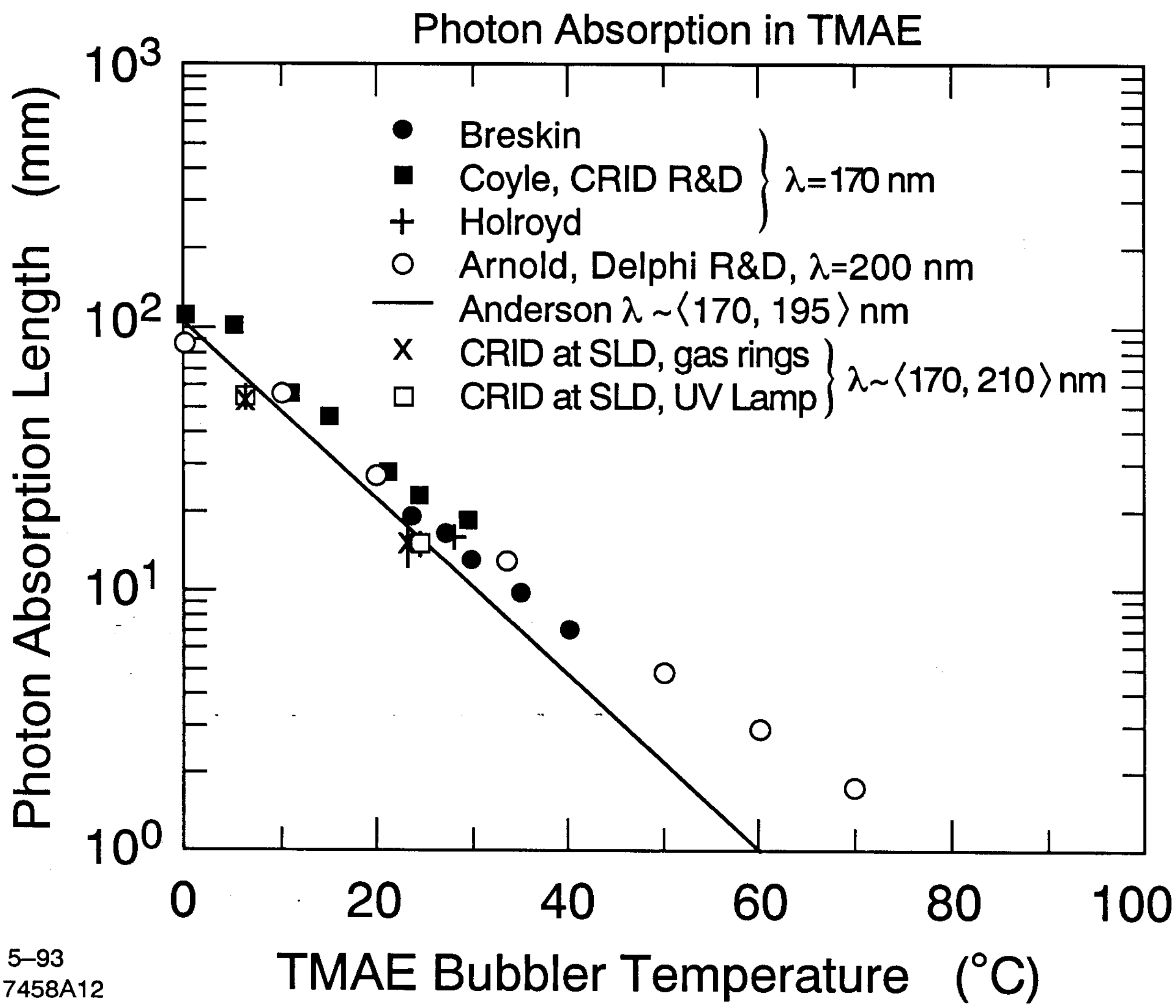
Photon Absorption in TMAE
10^3
10^2
10^1
10^0
Photon Absorption Length (mm)
● Breskin
■ Coyle, CRID R&D
+ Holroyd
λ=170 nm
○ Arnold, Delphi R&D, λ=200 nm
— Anderson λ ~⟨170, 195⟩ nm
X CRID at SLD, gas rings
□ CRID at SLD, UV Lamp
λ~⟨170, 210⟩ nm
0
20
40
60
80
100
TMAE Bubbler Temperature (°C)
5–93
7458A12

Fig. 15

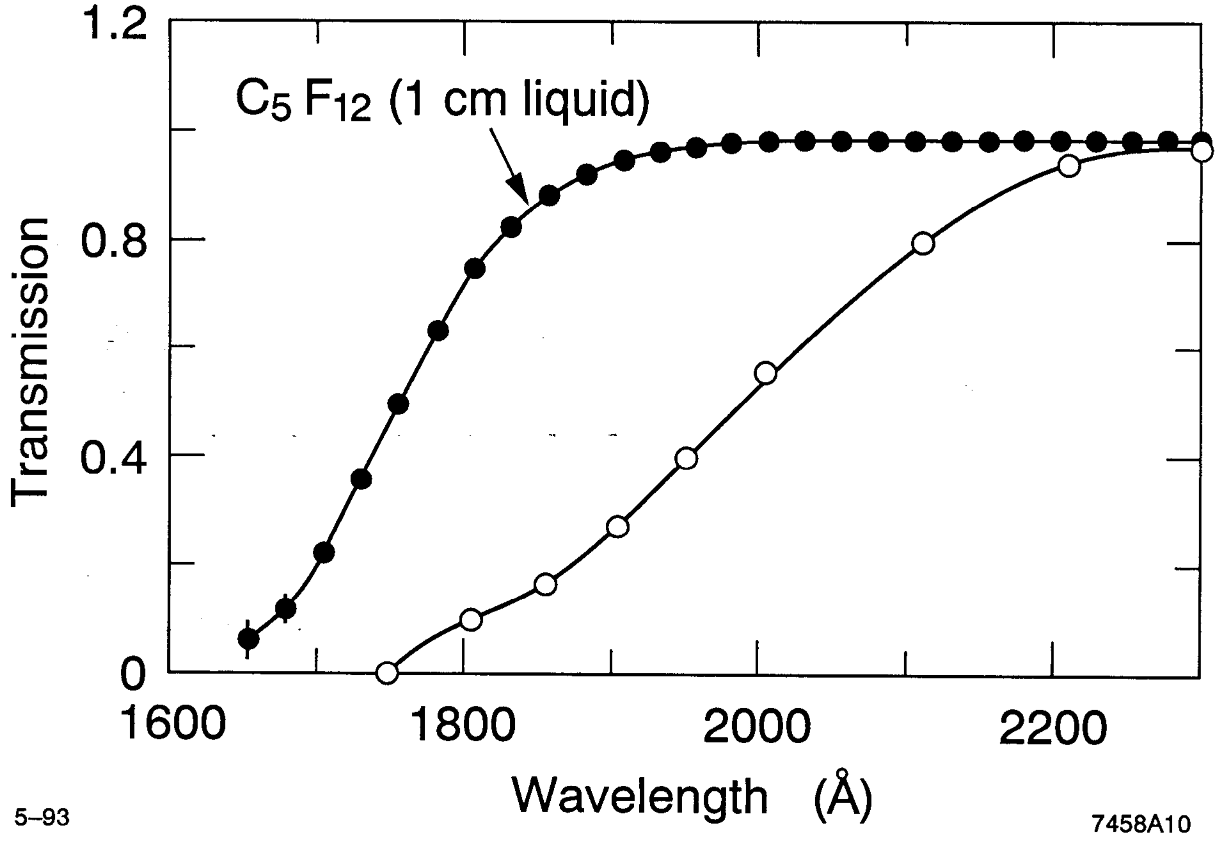
1.2
0.8
0.4
0
Transmission
$C_5 F_{12}$ (1 cm liquid)
1600
1800
2000
2200
Wavelength (Å)
5–93
7458A10

Fig. 16

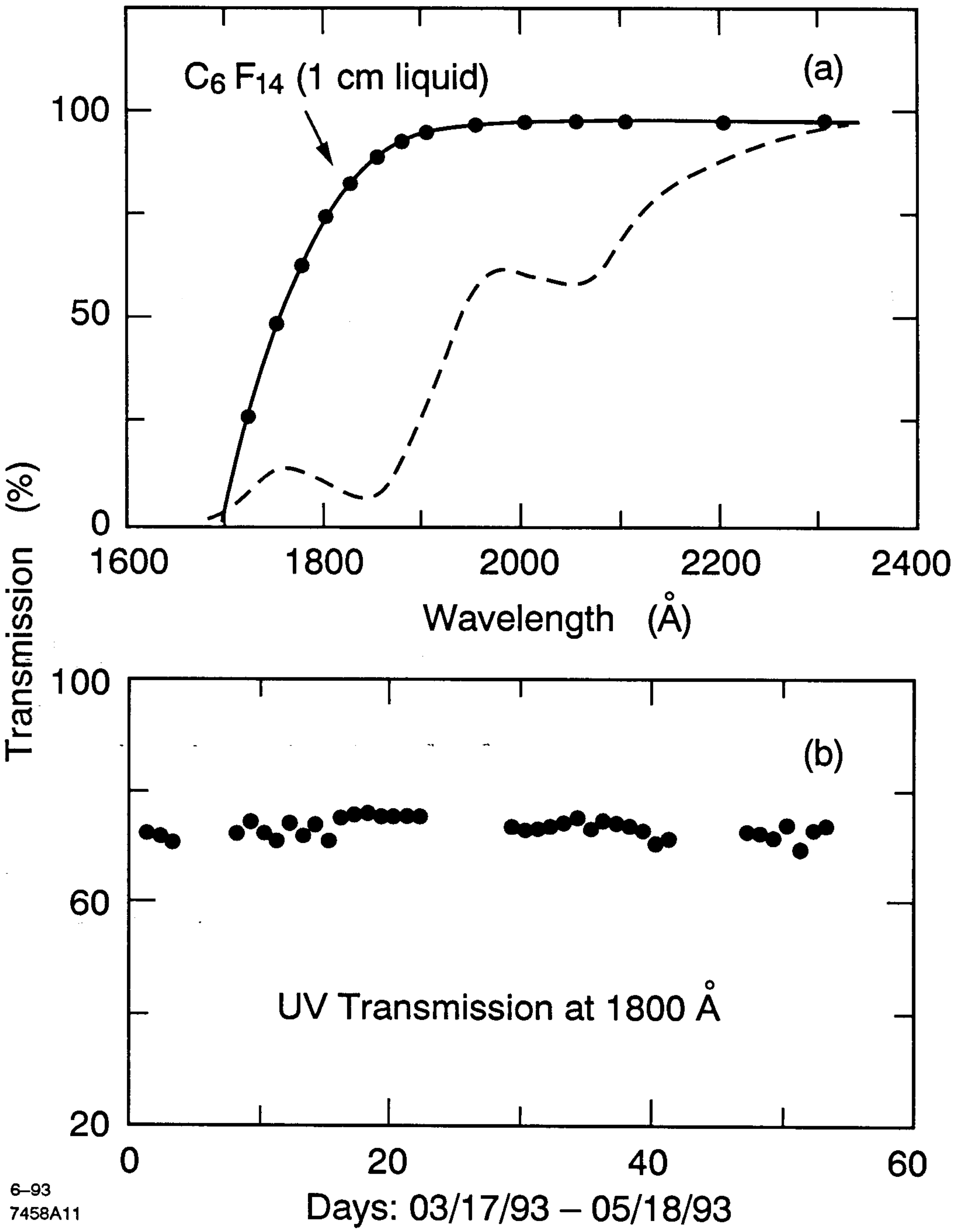

C_6F_{14} (1 cm liquid)
(a)
Transmission (%)
100
50
0
1600
1800
2000
2200
2400
Wavelength (Å)
100
(b)
60
UV Transmission at 1800 Å
20
0
20
40
60
6–93
7458A11
Days: 03/17/93 – 05/18/93

Fig. 17

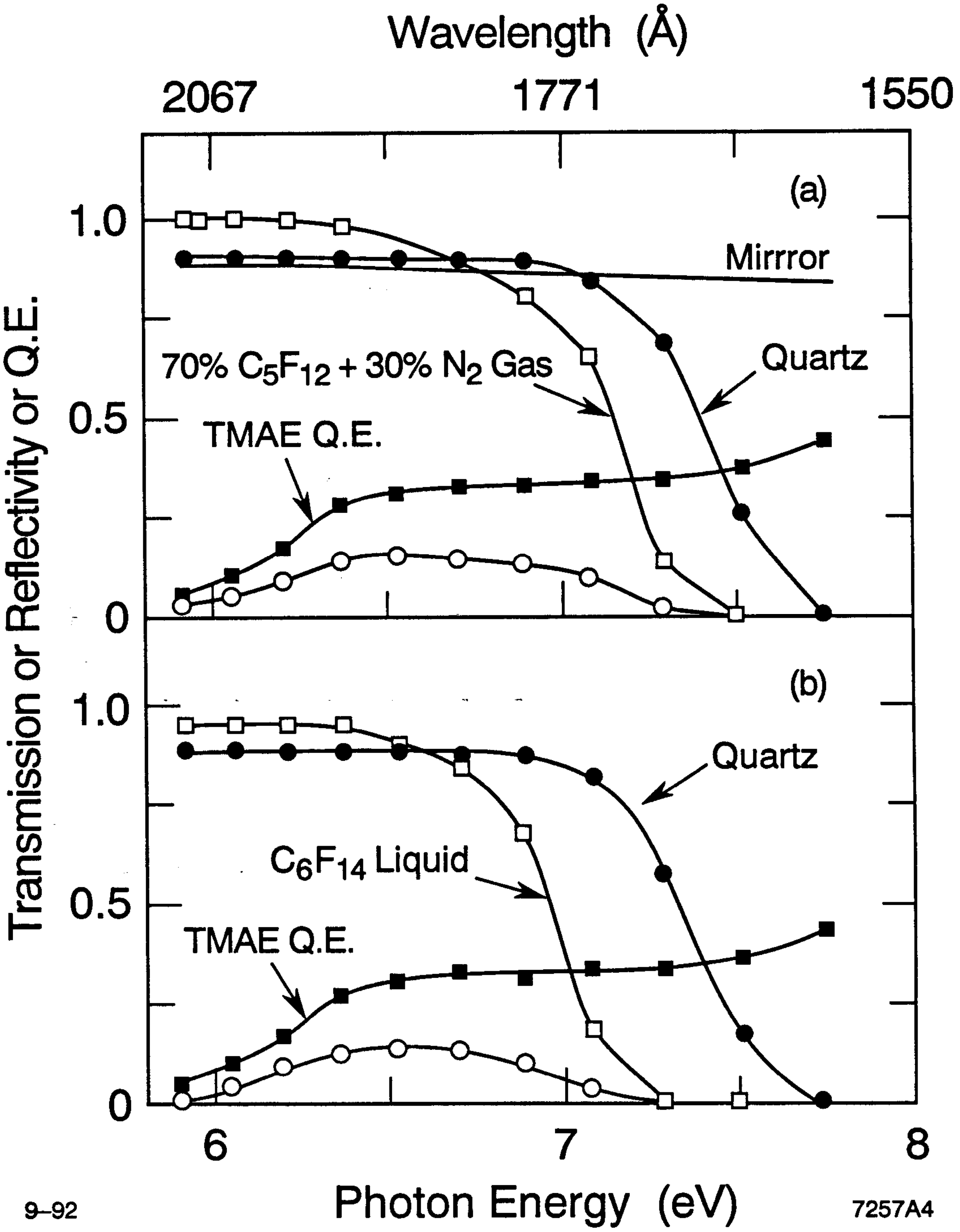
Wavelength (Å)
2067
1771
1550
(a)
1.0
0.5
0
Mirrror
Quartz
70% C_5F_{12} + 30% N_2 Gas
TMAE Q.E.
(b)
1.0
0.5
0
Quartz
C_6F_{14} Liquid
TMAE Q.E.
Transmission or Reflectivity or Q.E.
6
7
8
Photon Energy (eV)
9–92
7257A4

Fig. 18

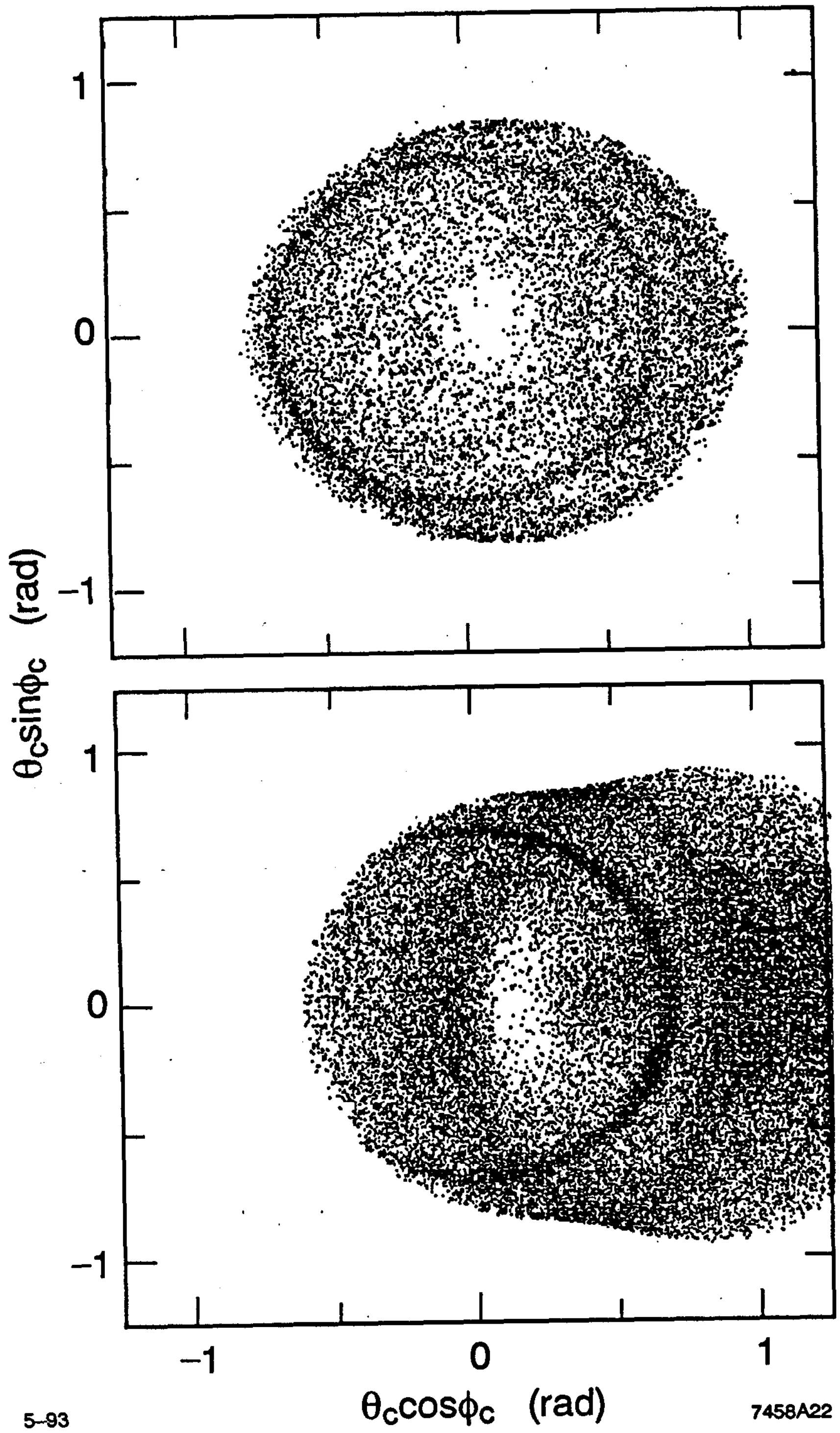

Fig. 19

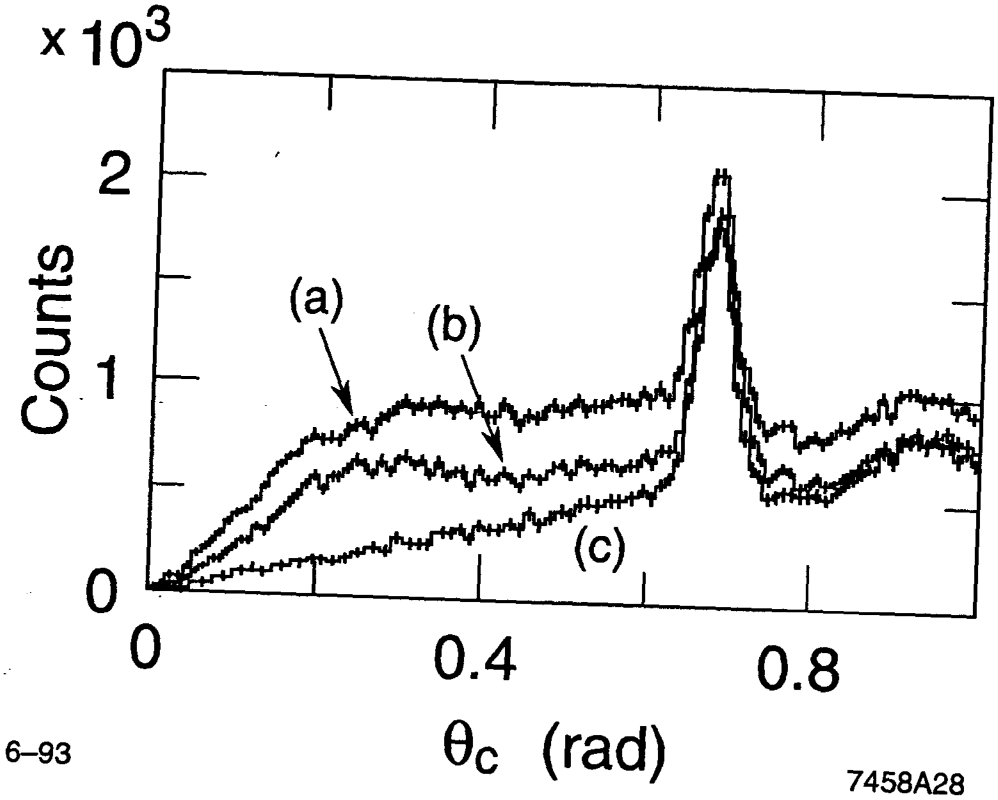

Fig.20

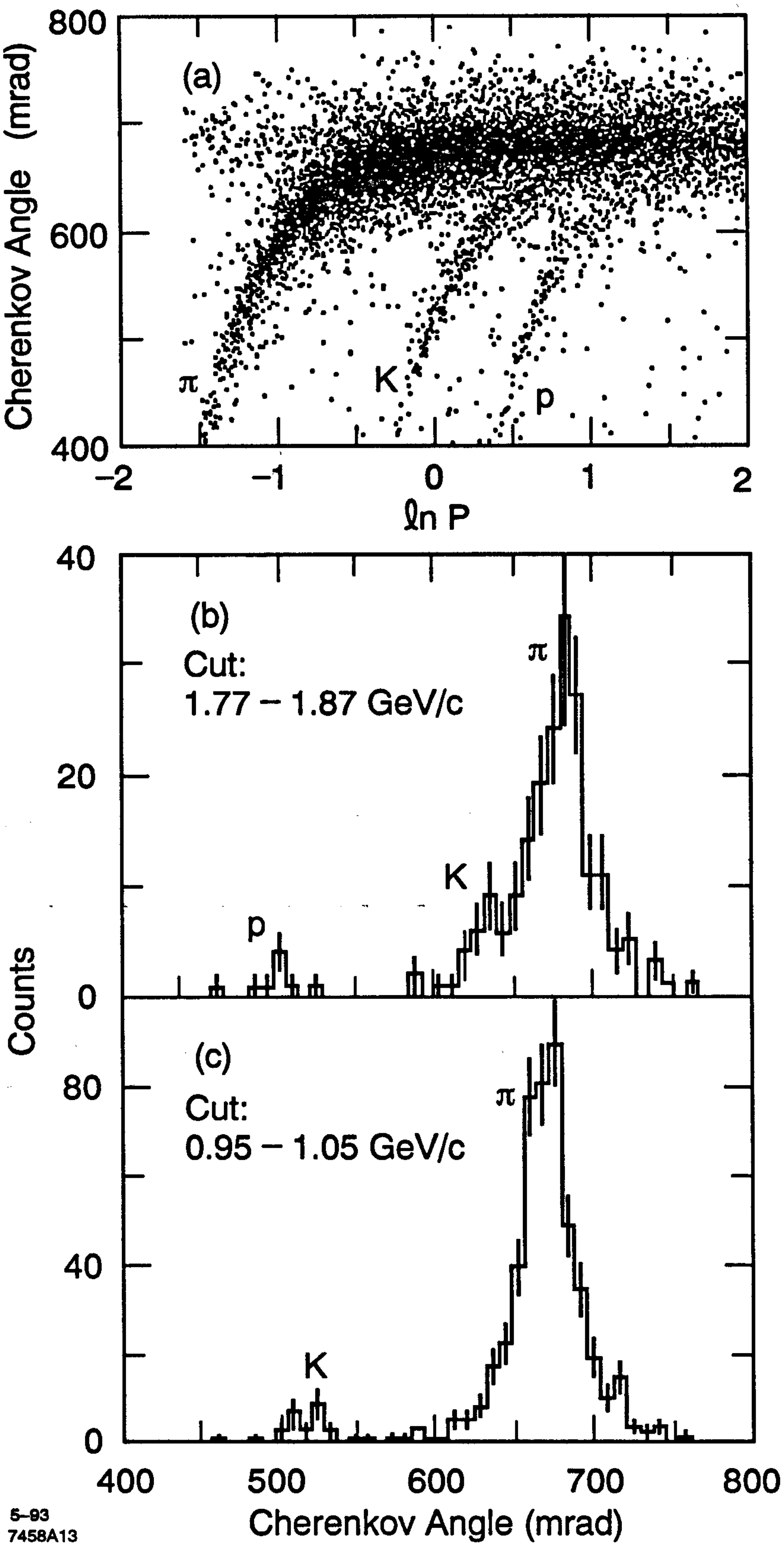
(a)
Cherenkov Angle (mrad)
800
600
400
π
K
p
−2
−1
0
1
2
ℓn P
(b)
Cut:
1.77 − 1.87 GeV/c
π
K
p
40
20
0
Counts
(c)
Cut:
0.95 − 1.05 GeV/c
π
K
80
40
0
400
500
600
700
800
Cherenkov Angle (mrad)
5–93
7458A13

Fig. 21

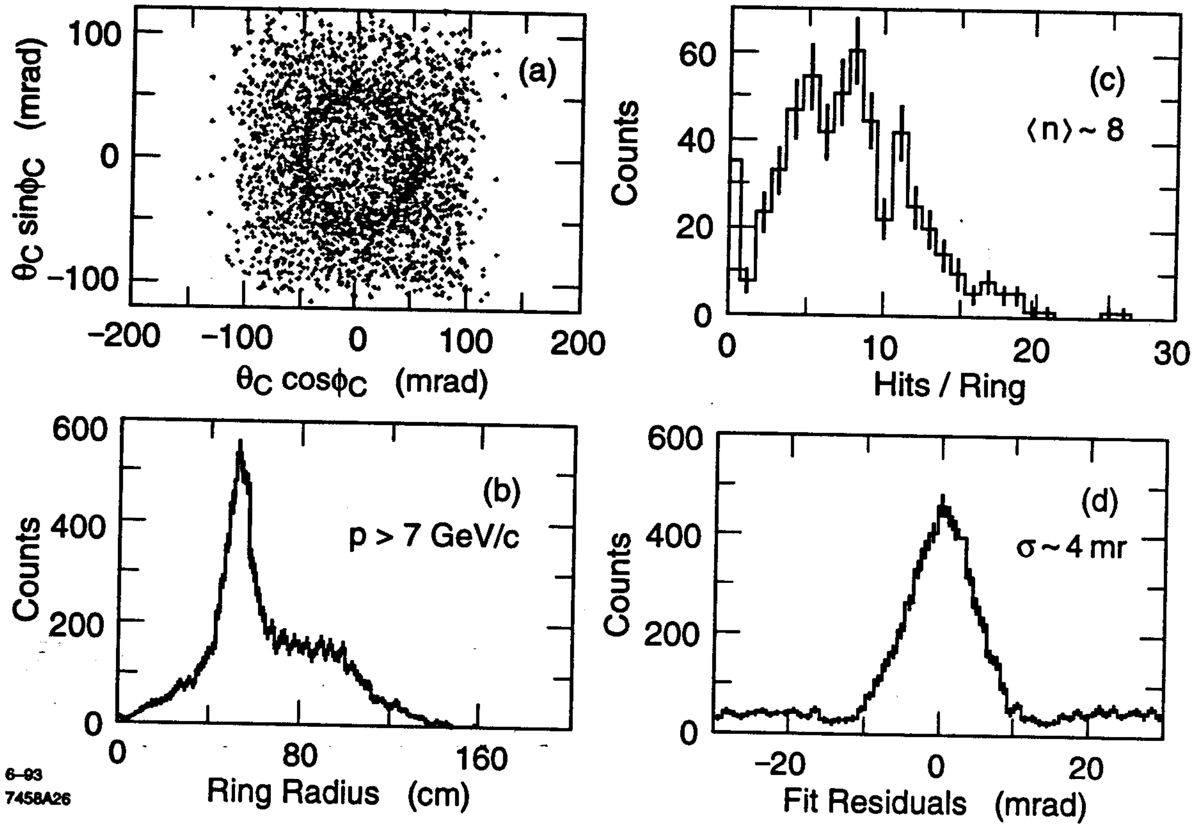
θC sinϕC (mrad)
100
0
−100
−200
−100
0
100
200
θC cosϕC (mrad)
(a)
Counts
60
40
20
0
0
10
20
30
Hits / Ring
(c)
⟨n⟩ ~ 8
Counts
600
400
200
0
0
80
160
Ring Radius (cm)
(b)
p > 7 GeV/c
6–93
7458A26
Counts
600
400
200
0
−20
0
20
Fit Residuals (mrad)
(d)
σ ~ 4 mr

Fig.22